Quaternary Research 84 (2015) 21–36

Contents lists available at ScienceDirect

Quaternary Research

journal homepage: www.elsevier.com/locate/yqres

Late Holocene precipitation variability recorded in the sediments of Reloncaví Fjord (41°S, 72°W), Chile

Lorena Rebolledo [a,b,c,*], Carina B. Lange [a,b,c], Sébastien Bertrand [d], Práxedes Muñoz [e], Marco Salamanca [c,f], Pablo Lazo [c], José L. Iriarte [b,g], Gabriel Vargas [h], Silvio Pantoja [a,b,c], Laurent Dezileau [i]

[a] Centro de Investigación Oceanográfica en el Pacífico Sur-Oriental (COPAS), Universidad de Concepción, Chile
[b] Programa COPAS Sur-Austral, Universidad de Concepción, Chile
[c] Departamento de Oceanografía, Universidad de Concepción, Chile
[d] Renard Centre of Marine Geology, Ghent University, Belgium
[e] Departamento de Biología Marina, Facultad de Ciencias del Mar, Centro de Estudios Avanzados en Zonas Áridas (CEAZA), Universidad Católica del Norte, Coquimbo, Chile
[f] Programa de Monitoreo del Ambiente Marino (PROMNA), Universidad de Concepción, Chile
[g] Instituto de Acuicultura, Universidad Austral de Chile, Sede Puerto Montt, Chile
[h] Departamento de Geología, Facultad de Ciencias Físicas y Matemáticas, Universidad de Chile, Chile
[i] Université de Montpellier 2, 34095 Montpellier cedex 05, France

ARTICLE INFO

Article history:
Received 28 September 2014
Available online 12 June 2015

Keywords:
Reloncaví Fjord
Patagonia
Geochemistry
Diatoms
Organic carbon
Stable isotopes

ABSTRACT

We present reconstructions of late Holocene changes in the source of organic matter and siliceous export production in the Relocanví Fjord (41°S, 72°W), Northern Chilean Patagonia, based on organic carbon content, $\delta^{13}C_{org}$, N/C ratio, diatom assemblages and biogenic silica contents from three sediment cores. The age models are based on a combination of ^{210}Pb profiles, AMS ^{14}C dating, and on the first occurrence of the diatom *Rhizosolenia setigera* f. *pungens*, as a stratigraphic marker in the fjords. The cores span the last 300 to 700 yr. Diatoms dominate the siliceous assemblages in the three cores (98% on average). Our results suggest that precipitation seasonality in the region of Reloncaví was high in CE 1300–1400 and CE 1700–1850, with a clear decreasing trend since CE 1850. The latter trend is in agreement with instrumental records and tree-ring reconstructions. These fluctuations seem to be associated with the Southern Annular Mode (SAM).

Introduction

The fjord system of Chilean Patagonia (41–55°S) is under the permanent influence of the Southern Westerly Winds (SWW), which are responsible for the high precipitation (1000–7000 mm yr^{-1}; e.g., Garreaud et al., 2013) on the western side of the Andes. The SWW display a marked seasonality: during winter, the core of the SWW migrates north and the wind belt expands latitudinally whereas in summer the SWW belt contracts and is centered south of 45° S with maximum precipitation in southernmost Patagonia (e.g., Garreaud et al., 2013).

Strong density, temperature and salinity gradients characterize the water column within the fjords, due to the mixing of relatively fresh surface waters from precipitation, river discharge and melting glaciers (0–30 m depth, offshore flow) with saltier Pacific subantarctic waters (down to ~150 m depth, onshore flow) (e.g., Sievers and Silva, 2008). The biological productivity of the Chilean fjords is influenced by the combined effect of important contributions of dissolved silicon from freshwater discharge as well as the vertical entrainment of subantarctic waters rich in macronutrients (nitrate and orthophosphate) from the adjacent oceanic area (Iriarte and González, 2008; González et al., 2010; Vargas et al., 2011). High seasonal variability in primary production and solar radiation characterize the Patagonian fjord system (Acha et al., 2004; Iriarte et al., 2007; González et al., 2010; Montero et al., 2011).

Patagonian fjord sediments are mostly composed of a mix of marine and terrestrial sources; the latter includes allochthonous organic matter (OM) and lithogenic particles. The proportion of lithogenic particles is generally higher at the heads of the fjords than in the oceanic area, due to local runoff (Sepúlveda et al., 2011; Silva et al., 2011; Vargas et al., 2011; Bertrand et al., 2012a; Montade et al., 2012). In glacier-influenced fjords, sediments have a very low OM content due to dilution by large amounts of inorganic matter (i.e., glacial clay) originating from glacier erosion (Silva and Prego, 2002; Silva et al., 2011). Both freshwater and marine diatoms are abundant in fjord sediments, allowing reconstructions of variability in freshwater input (tied to precipitation on land and river runoff into the fjords) and siliceous productivity through time (e.g., Sepúlveda et al., 2005; Rebolledo et al., 2011).

In the past decade, paleoclimate studies in the Chilean fjord area have increased significantly and new knowledge on paleotemperature as well as changes in SSW strength and related precipitation has been

* Corresponding author at: Centro de Investigación Oceanográfica en el Pacífico Sur-Oriental (COPAS), Universidad de Concepción, Chile.
E-mail address: lrebolle@udec.cl (L. Rebolledo).

http://dx.doi.org/10.1016/j.yqres.2015.05.006
0033-5894/

gained. Recently, Kilian and Lamy (2012) and Kilian et al. (2013) have provided comprehensive reviews of continental paleoclimate and marine paleoproductivity changes in the southernmost Patagonian region, based on fjord and lake sediments, peat bogs, and stalagmites. In Northern Patagonia, numerous terrestrial pollen records from peat bogs, lake and fjord sediments have been used to reconstruct past vegetation and climate changes during the Holocene (e.g., Jara and Moreno, 2012; Montade et al., 2012). A recent study by Bertrand et al. (2014a) suggested that changes in wind-driven precipitation co-varied with sea surface temperature in northern Chilean Patagonia over the last 1400 yr, with a northward migration of the wind belt during cold phases and vice versa. However, few works have used a multi-proxy approach (e.g., Rebolledo et al., 2008; Sepúlveda et al., 2009; Fletcher and Moreno, 2012), and little information exists on the variability of precipitation, runoff and terrigenous organic carbon contents preserved in sedimentary cores of Northern Patagonia during the last 2000 yr. Within the last ~2000 yr two climate/productivity regimes were inferred from sedimentary multi-proxy studies in the Jacaf Fjord (44°S, 73°W): dry/warm climate and decreased marine productivity before CE 1050, and wet/cold climate and increased productivity after CE 1200 (Rebolledo et al., 2008; Sepúlveda et al., 2009). Recent sedimentary records encompassing the past 150 yr in the Puyuhuapi Channel (44°S, 70°W) and Gulf of Ancud (42°S, 72°W) have shown a decreasing trend in the terrestrial signal (i.e., freshwater diatoms) during the 20th century associated with a decrease in precipitation/river runoff and the occurrence of El Niño events (Rebolledo et al., 2005, 2011). Diminished precipitation and river discharge over the last 400 yr have also been derived from dendrochronological studies in Northern Patagonia (Lara et al., 2008; Villalba et al., 2012).

In Patagonian fjord sediments, fluctuations in the sources of organic matter (OM), as calculated from $\delta^{13}C_{org}$ stable isotopes and the contents of freshwater diatoms preserved in sediments have been used as proxies for precipitation and river discharge (e.g., Rebolledo et al., 2005, 2011; Sepúlveda et al., 2009; Mayr et al., 2014).

The Northern Patagonia fjords are located at the northern limit of the strongest influence of the SWW and thus the area is ideally located to reconstruct past changes in precipitation-driven continental runoff and sources of OM. The sediments are characterized by high deposition rates of both marine and terrestrial material (e.g., Sepúlveda et al., 2009; Aracena et al., 2011; Silva et al., 2011). Thus, it is important to establish reliable proxies of changes in precipitation and sources of OM preserved in the sediments of the Chilean fjords, where the instrumental records are limited (i.e., restricted to a few locations), sometimes discontinuous, and cover only the last ca. 150 yr.

Existing studies of Reloncaví Fjord (41°S, 72°W) focus on the geochemistry of the surface sediments (Silva et al., 2009, 2011), the geomorphology of the fjord (Araya–Vergara et al., 2008), sedimentary evidences of paleo-earthquakes (St-Onge et al., 2012), and assessments of the impacts of aquaculture (Iriarte et al., 2010). None of these studies uses a multi-proxy approach combining changes in siliceous microfossils (mainly freshwater diatoms) and geochemistry to reconstruct past climate and environmental changes through time. Our objectives were: 1) to study the spatial variability in geochemical features of the Reloncaví Fjord, and 2) to provide a ~700-yr history of past variability in siliceous export production and OM sources (terrigenous and marine) related to changes in precipitation and river discharge to the fjord.

Study area

The Reloncaví Fjord, located in Northern Patagonia (41° 21′ to 41° 45′S; 72° 16′ to 72° 39′ W, Fig. 1), is ~55 km long and 3 km wide, with depths ranging from 450 m near the mouth (opening to the large Reloncaví Sound without a well-defined sill) to <100 m at its head (Valle-Levinson et al., 2007; Castillo et al., 2012). This fjord provides important ecosystem services as it is intensely used for tourism and aquaculture (salmonids, mytilids) that has resulted in an important anthropogenic intervention since CE 1980 (Iriarte et al., 2010).

Climate, oceanography and plankton

Precipitation in the area fluctuates between 1800 and 3400 mm yr^{-1} with maxima in austral winter. At 41°S, precipitation is almost entirely controlled by the SWW and there is a strong correlation between zonal wind velocity and precipitation ($r = 0.8$; Garreaud et al., 2013). The latitudinal position of the SWW belt is strongly related to atmospheric and sea surface temperature, on various time scales (Lamy et al., 2010). When the climate is colder, the westerlies migrate toward the equator and vice versa. In the first case, precipitation seasonality is low (it rains all year instead of just in winter) and/or there is more precipitation depending on the latitude. In contrast, when the SWW are in a southernmost position, precipitation seasonality is high (i.e., wet winters and very dry summers). This is when erosion and transport of terrestrial organic matter toward the fjords increase (Bertrand et al., 2014a).

Freshwater supply into the Reloncaví Fjord comes mainly from the Puelo (annual average 650 m^3 s^{-1}), Petrohué (280 m^3 s^{-1}) and Cochamó (35 m^3 s^{-1}) rivers (Valle-Levinson et al., 2007; Iriarte et al., 2010; http://www.dga.cl) (Fig. 1). These rivers have pluvial–nival regimes with maximum discharges during winter (May through August) and a secondary peak associated with snow meltwater in spring (November to early December; Castillo et al., 2012).

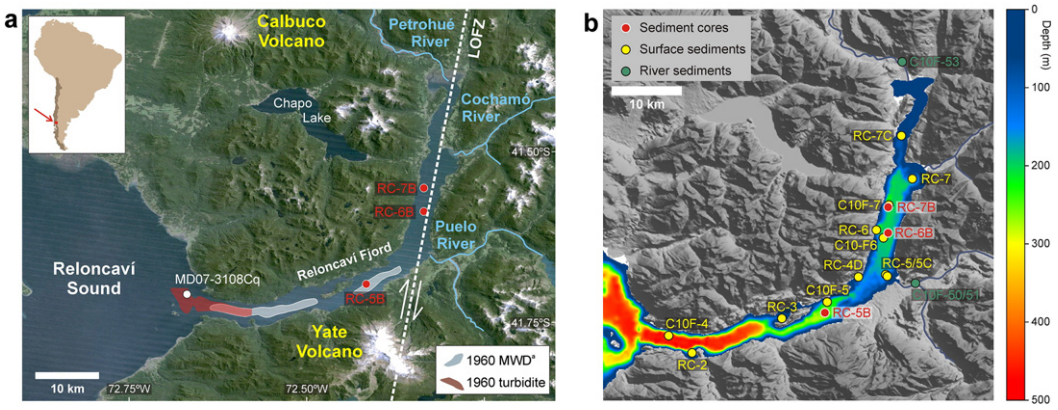

Figure 1. General map of the Reloncaví Fjord. (a) Satellite image of the study area with indication of the main river inflows. The approximate trace of the Liquiñe-Ofqui Fault Zone (LOFZ) is drawn according to Adriasola and Stöckhert (2008). The location of the 1960 turbidite and Mass-Wasting Deposits (MWD) are from St-Onge et al. (2012). Note that the 1960 turbidite is restricted to the outer basin and that core RC-5B is located at the outer edge of the 1960 mass-wasting deposit. (b) Sampling locations are indicated on the bathymetric map of Reloncaví Fjord (from Castillo et al., 2012). See Table 1 for the exact coordinates.

Reloncaví Fjord is highly stratified. This is particularly evident in salinities of the fjord, which vary between 3 and 32.6 psu, with values <20 psu at 0–5 m, and higher salinities at depth (Castillo et al., 2012). Lowest salinities are found within the first few meters of the water column at stations near the mouths of the Petrohué, Puelo and Cochamó rivers. Water temperatures in winter and austral spring vary between 10.5 and 16°C with highest values within the first 20 m of the water column. Dissolved oxygen concentrations are 9–8 mL/L at the surface, and lower at depth but never below 2 mL/L. Silicic acid ranges 50 (surface) to 3 μM (bottom) from surface to bottom and the highest values are found close to the discharge of the main rivers and in the Marimelli basin. Nitrate and orthophosphate concentrations are the lowest at the surface, reflecting consumption by phytoplankton in surface layers, and increase with depth (concentrations ranges are: 0.5–27 μM for nitrate and 0.3–2.8 μM for orthophosphate). Water column data can be found at http://www.shoa.cl/n_cendhoc/productos/cimar10/area/web_areaestudio.html.

Phytoplankton distribution in the Reloncaví Fjord follows a clear succession with large (>20 μm) chain-forming diatoms dominating in spring with blooms of *Chaetoceros didymus*, *C. radicans*, *C. convolutos*, *Leptocylindrus danicus*, *Rhizosolenia* spp. and *Skeletonema* spp. followed by thecate dinoflagellates in winter (Iriarte and González, 2008; González et al., 2010). Maximum values of primary production (0.4–3.8 g C m^2 d^{-1}) are observed during austral spring to late summer and minimum values in winter (0.1–0.2 g C m^2 d^{-1}) (Montero et al., 2011).

Geology

The Reloncaví Fjord basin is mostly composed of granodiorites that belong to the Northern Patagonian batholith, and Quaternary volcanic rocks (SERNAGEOMIN, 2003). The bedrock is locally covered by Quaternary glacio-fluvial deposits and easily erodible postglacial volcanic ash soils (Bertrand and Fagel, 2008). The upper basin of the Reloncaví Fjord between the Petrohué and Puelo deltas, follows the Liquine-Ofqui Fault Zone (Fig. 1a), which is a major transpressional system with associated Quaternary volcanoes (Lange et al., 2008; Cembrano and Lara, 2009), along which earthquakes ruptures (e.g., the last 2007 Moment magnitude (M_w) 6.2 event; Legrand et al., 2011; Vargas et al., 2013) trigger landslides on land, in lakes and in the fjords (Chapron et al., 2006; Watt et al., 2009; St-Onge et al., 2012; Van Daele et al., 2013). In addition, large subduction earthquakes affected the area in CE 2010 (M_w 8.8), CE 1960 (M_w 9.5), CE 1837, CE 1737, and CE 1575; all of them, except for the CE 1737 event, were related to very long rupture zones and were capable of generating tsunamis in some of the fjords and in the adjacent Pacific Ocean (e.g., Cisternas et al., 2005; St-Onge et al., 2012). Earthquake-triggered mass-wasting deposits were also identified on seismic profiles acquired along the slopes of the Puelo River delta and in the infill of the intermediate and outer basins (St-Onge et al., 2012). Additionally, four active volcanoes (Calbuco, Yates, Osorno and Hornopirén; Fig. 1a) are located in the vicinity of the Reloncaví Fjord (Fontijn et al., 2014). Edifice collapse generating landslides are a major hazard posed by many volcanoes (e.g., Watt et al., 2009).

Materials and methods

Sampling

We recovered eleven surface fjord sediment samples (0–1 cm) corresponding to sites that follow a gradient from the mouth to the head of the fjord (Fig. 1b). These sediments were recovered with a Rumohr corer (RC) during the campaigns of 2008 and 2009 onboard L/C Tirana, and in 2012 onboard RV Jürgen Winter. Additionally, we make use of geochemical information previously obtained by Silva et al. (2009, 2011) from fjord surface sediments (stations C10F-4, C10F-5, C10F-6 and C10F-7), as well as from local rivers Puelo and Petrohué (stations C10F-50, C10F-51, C10F-53; Table 1 and Fig. 1b), which were collected in 2004 during the CIMAR-10 FIORDOS cruise (http://www.shoa.cl/n_cendhoc/productos/cimar10/index.html).

Analytical results from surface sediment samples were plotted to visualize spatial distribution of geochemical variables using Ocean Data View (ODV) Software version 4.6.1. The graphic representation of the data was constructed with a VG gridding.

Cores were collected with a Rumohr corer at three sites (RC-5B, RC-6B and RC-7B) in the Reloncaví Fjord in November 2008 onboard the L/C Tirana (Fig. 1b; Table 1). The ca. 75-cm long cores were extruded and sliced at 1-cm intervals. The samples were stored in plastic bags and kept frozen at −20°C until laboratory analyses on land. For certain strata, smear-slides were taken following the procedure of Mazzullo et al. (1988) and analyzed under the light microscope.

Physical properties of the sediment

Dry bulk density (DBD) was calculated as:

$$\mathrm{DBD}(\mathrm{g\ cm^{-3}}) = \mathrm{dry\ mass(g)}/\left[(\mathrm{dry\ mass\ (g)}/2.65\ \mathrm{g\ cm^{-3}}) + (\mathrm{water\ mass\ (g)}/1.025\ \mathrm{g\ cm^{-3}})\right],$$

where 2.65 g cm^{-3} is the grain density and 1.025 is the density of fjord water (Bloesch and Evans, 1982).

Magnetic susceptibility was determined every 1 cm using a Bartington MS2E sensor connected to a Bartington MS2 meter. Results are expressed as 10^{-8} dimensionless (SI) volume-susceptibility units. Measurements were performed at the Sedimentology Laboratory of the EULA Center, University of Concepción, Chile. Grain size analysis was performed on wet sediments using a Malvern Mastersizer 2000 equipped with a Hydro-G dispersion unit at the Laboratory of Sedimentology of the University of Chile, Santiago. Proportions of clay, mud and sand and other statistical parameters of the grain size distributions (mean grain size, skewness, sorting, and kurtosis) were calculated with the statistical software Gradistat version 8.0 using the geometric moments method (Blott and Pye, 2001).

Age–depth modeling

The chronology of the three cores was established by combining ^{210}Pb measurements, ^{14}C dating, and the first occurrence of the diatom *Rhizosolenia setigera* f. *pungens* (Cleve-Euler) Brunel 1962, which has been previously used as a marker for ~CE 1898–1919 in the Ancud Gulf (Rebolledo et al., 2011). ^{210}Pb concentrations were measured by alpha spectrometry of its daughter isotope ^{210}Po (in secular equilibrium), using an Ortec Alpha Spectrometer at the laboratory Géosciences of the Université de Montpellier, France (see Rebolledo et al., 2011 for methodology details). ^{210}Pb ages were estimated using the Constant Rate Supply model (CRS, Appleby and Oldfield, 1978; Turekian et al., 1980; Cochran et al., 1998), which assumes a constant flux of $^{210}Pb_{xs}$ to the sediments, and allows determination of recent sedimentation rates and ages.

A total of 13 AMS ^{14}C ages was obtained on bulk sedimentary organic matter (n = 10), organic (n = 2; plant, wood) and inorganic (n = 1; marine shell fragment) macro-remains picked from the three sediment cores (Table 2). No terrestrial macro-remains suitable for dating were found in cores RC-5B and RC-6B. Radiocarbon concentrations were measured at the National Ocean Sciences Accelerator Mass Spectrometry (NOSAMS) Facility and Beta Analytics, USA. Radiocarbon ages were calibrated using the calibration curve SHCal04 (McCormac et al., 2004). A correction of 360 yr was applied to all ^{14}C ages obtained on bulk sediment. This value was calculated as the difference between ^{14}C ages results obtained on terrestrial organic macro-remains (Beta-326985 and Beta-326987) and bulk sediments (OS-73586 and OS-73587) in sediment core RC-7B (Table 2). This correction assumes

Table 1
Location of sampling sites and geochemical data obtained from surface sediments in the Reloncaví Fjord.

Numbers	Sampling sites	Latitude (°S)	Longitude (°W)	Water depth (m)	Si_{OPAL} (%)	C_{org} (%)[a]	N_{tot} (%)	N/C	$\delta^{13}C_{org}$
	Surface sediment samples								
1	RC-2	−41.739	−72.586	210	4.77	0.24	0.05	0.17	−22.92
2	RC-3	−41.695	−72.471	118	10.46	1.76	0.20	0.10	−22.98
3	RC-5B	−41.686	−72.416	260	8.12	1.06	0.09	0.08	−22.30
4	RC-4D	−41.642	−72.373	91	4.63	1.26	0.12	0.08	−24.47
5	RC-5	−41.641	−72.336	152	8.52	2.31	0.14	0.05	−26.40
6	RC-5C	−41.639	−72.338	174	9.66	2.80	0.15	0.05	−27.15
7	RC-6	−41.582	−72.350	141	8.65	1.54	0.13	0.07	−24.97
8	RC-6B	−41.584	−72.335	196	7.65	1.78	0.22	0.11	−22.97
9	RC-7B	−41.551	−72.335	200	7.24	1.06	0.82	0.07	−22.94
10	RC-7	−41.514	−72.304	117	10.24	1.77	0.16	0.08	−25.14
11	C10F-7	−41.550	−72.334	196	6.37	1.20	0.13	0.09	−24.20
12	RC-7C	−41.459	−72.318	90	6.35	1.78	0.25	0.10	−25.43
13	C10F-4[a]	−41.717	−72.616	452	6.56	1.0	0.10	0.09	−24.50
14	C10F-5[a]	−41.674	−72.413	175	6.01	1.2	0.14	0.10	−24.50
15	C10F-6[a]	−41.592	−72.341	155	5.78	1.4	0.14	0.10	−23.70
	River sediment samples								
16	C10F-50[b]	−41.650	−72.300	0		2.5	0.17	0.06	−24.30
17	C10F-51[b]	−41.650	−72.300	0		3.6	0.25	0.08	−26.40
18	C10F-53[b]	−41.367	−72.317	0		9.3	0.74	0.07	−25.90

[a] Data from cruise CIMAR-10 FIORDOS (Silva et al., 2009, 2011; www.cendhoc.cl).
[b] Riverine samples (Silva et al., 2011).

that the ^{14}C results obtained on organic macro-remains represent the real age of deposition. Since carbon in the bulk sediment samples originates from both marine and terrestrial sources, the correction of 360 yr combines the local marine reservoir effect (480–530 yr; Mohtadi et al., 2007; Bertrand et al., 2012b) and the soil carbon sequestration effect (i.e., the age of terrestrial carbon reaching the fjords is older than the age of deposition; Bertrand et al., 2012c).

The final age models were constructed with the software CLAM 2.1 (Blaauw, 2010), using the ^{210}Pb CRS ages, the first occurrence of *Rhizosolenia setigera* f. *pungens* and the calibrated ^{14}C ages (Table 2). Smooth splines (smooth level 0.75) were fitted through the datapoints, taking into account the instantaneous deposition of the sand layers. Three ^{14}C ages were considered as outliers based on their stratigraphic position and on their anomalous ages compared to the surrounding samples (Table 2). Since no detailed sedimentological core description was available, only the sand layers were considered as event deposits when constructing the age–depth models. Non-sandy turbidites related to large subduction earthquakes of Valdivia (1960 and CE 1575) may however occur in some of the cores (e.g., Chapron et al., 2006; St-Onge et al., 2012). Finally, the age distributions of the sand layers were computed using CLAM 2.1.

Geochemical analyses

Determination of biogenic silica followed the methodology described by Mortlock and Froelich (1989) and was conducted at the laboratories of Marine Organic Geochemistry and Paleoceanography, University of Concepción, Chile. Values are expressed as Si_{OPAL} (%) and measured with an analytical precision of ±0.5%. Because diatoms are the main component of the siliceous assemblage in Northern Patagonian fjords (e.g., González et al., 2010), we use the content of biogenic silica in our cores as a proxy for siliceous export production (see review in Tréguer and De La Rocha, 2013).

Table 2
AMS ^{14}C ages obtained on sediment cores RC-5B, RC-6B and RC-7B from the Reloncaví Fjord. The ^{14}C ages were calibrated with OxCal 4.1.5, using the SHCal04 calibration curve (McCormac et al., 2004). A reservoir correction of 360 yr was applied to the bulk sediment samples (see details in age–depth modeling section). Asterisks indicate ages that were not included in the final age models. The first two samples of core RC-5B were considered as outliers, based on their stratigraphic position immediately above and below a sand layer, which means that they likely reworked material. Likewise, the mollusk sample from core RC-6B (60–61 cm) was rejected because of its anomalously old age, which may be related to the lack of constraints on reservoir ages in the Chilean fjords.

Core number	Depth in core (cm)	Laboratory code	Material	$\delta^{13}C_{org}$ (‰)	^{14}C age (^{14}C yr BP ± 1σ)	Calibrated ages (cal yr CE)		Calibrated ages after correction (cal yr CE)	
						2 σ range	Weighted average	2 σ range	Weighted average
RC-5B*	31–32	Beta-326982	Bulk organic matter	−24.7	1090 ± 30	898–1042	999	1258–1402	1359
RC-5B*	43–44	Beta-330350	Bulk organic matter	−25	1280 ± 30	690–886	796	1050–1246	1156
RC-5B	58–59	Beta-326983	Bulk organic matter	−24.6	1090 ± 30	898–1042	999	1258–1402	1359
RC-5B	64–65	Beta-330351	Bulk organic matter	−23.9	1010 ± 30	1021–1153	1089	1381–1513	1449
RC-6B	32–33	OS-73722	Bulk organic matter	−27.25	655 ± 30	1300–1401	1349	1660–1761	1709
RC-6B	59–60	Beta-326984	Bulk organic matter	−24.4	760 ± 30	1229–1382	1295	1589–1742	1655
RC-6B*	60–61	OS-73485	Mollusk	0.91	375 ± 30	1464–1632	1554		
RC-6B	71–72	OS-73585	Bulk organic matter	−26.95	1170 ± 40	782–1016	925	1142–1376	1285
RC-7B	30–31	Beta-326985	Wood	−27.9	160 ± 30	1674–1954	1823		
RC-7B	45–46	Beta 326986	Bulk organic matter	−25.9	690 ± 30	1290–1392	1341	1650–1752	1600
RC-7B	45–46	OS-73586	Bulk organic matter	−27.25	470 ± 25	1428–1496	1459	1788–1856	1819
RC-7B	58–59	Beta-326987	Plant material	NA	210 ± 30	1649–1953	1763		
RC-7B	59–60	OS-73587	Bulk organic matter	−27.48	610 ± 25	1319–1421	1375	1679–1781	1735

For determination of organic carbon (C_{org}) and total nitrogen (N_{tot}) contents, ~100 mg of freeze-dried sediments were ground and sent for analysis to the Stable Isotopic Facility of the School of Biological Sciences, University of Washington, USA. The samples were acidified to remove inorganic carbon. The dry material (~30 mg) was placed in tin capsule and combusted in an Eurovector (Milan, Italy) elemental analyzer. The resulting CO_2 gas was separated by gas chromatography and analyzed in a Micromass (Manchester, UK) Isoprime isotope ratio mass spectrometer (IRMS). Carbon stable isotopes (δ^{13} C_{org}) were determined using the elemental analyzer coupled with a Mass Spectrometer, in Manchester, UK, with a precision ±0.27‰. $\delta^{13}C_{org}$ values are expressed as ‰ relative to the Pee Dee Belemnite (PDB) standard:

$$\delta^{13}C_{org}(‰) = \left[\left(^{13}C/^{12}C\right)_{sample}/\left(^{13}C/^{12}C\right)_{standard}-1\right] \times 1000$$

We use the N/C molar ratio to reflect the contribution of terrestrial organic carbon in marine environments (Perdue and Koprivnjak, 2007; Sepúlveda et al., 2011). δ^{13} C_{org} and the N/C ratio have been widely used as indicators of the source of OM, either allochthonous (terrestrial) or autochthonous (marine) (e.g., Thornton and McManus, 1994; Meyers, 1997; Perdue and Koprivnjak, 2007). We use these two proxies to help reveal past changes in the source of OM.

The relative contribution of allochthonous OM in cores RC-5B (located near the mouth of the Puelo River) and RC-6B and RC-7B (near the mouth of the Cochamó River) was assessed with the two-source mixing model of Thornton and McManus (1994), as:

$$\%\ \text{allochthonous material (terrestrial)} = \left[\left(\delta^{13}C_{org\ sample}-\delta^{13}C_{org\ marine}\right)/\left(\delta^{13}C_{org\ terr}-\delta^{13}C_{org\ marine}\right)\right] \times 100,$$

where % autochthonous material (marine) = 100 − % allochthonous (terrestrial) material; $\delta^{13}C_{org\ sample}$ = isotopic value of the sample; $\delta^{13}C_{org\ marine}$ = marine end member value −20.5‰ (Rebolledo et al., 2011) and $\delta^{13}C_{org\ terr}$ = terrestrial end member value −29.3‰ (Sepúlveda et al., 2011).

We estimated mass accumulation rates of terrigenous organic carbon ($MAR_{terr\ OM}$) from the % allochthonous material (see above) as follows:

$$MAR_{terr\ OM} = C_{org\ terr} \times DBD \times SR,$$

where $C_{org\ terr}$ is the concentration of terrigenous organic carbon in a given strata, DBD is the dry bulk density in g cm^{-3}, and SR is the sedimentation rate in cm yr^{-1} obtained from CLAM 2.1 software.

Siliceous microfossils counts

Cores RC-6B and RC-7B were used for identification and counts of diatoms, silicoflagellates, sponge spicules, crysophyte cysts and phytoliths, following Schrader and Gersonde (1978). Approximately 500 mg of freeze-dried sediments were oxidized using a mix of hydrogen peroxide at 30%, sodium pyrophosphate and hydrochloric acid to remove organic matter, clays and carbonates. Once the samples were cleaned, 0.2 ml was deposited onto a cover slip, air dried and mounted with Naphrax mounting medium (refraction index = 1.7). Two permanent slides per sample were prepared in this fashion and observed under a Zeiss Axiosocope 2 plus microscope with phase contrast at 400× and 1000×. For each sample, at least 300 diatom valves were counted. Diatom species identification was based on the works of Cupp (1943); Rivera (1981); Round et al. (1990); Hasle and Syvertsen (1996); Sims (1996) and Witkowski et al. (2000). Diatoms were grouped by ecological affinity into the following categories: high nutrient (HN), coastal planktonic (CP), non-planktonic (NP which groups benthic, epiphytic, epipsamic and tycoplanktonic species), freshwater (FW), warm water (WW), and cold water (CW) (Rebolledo et al., 2011). Laboratory and microscopy work was carried out at the Paleoceanography laboratory, University of Concepción.

We also calculated diatom diversity as the Shannon-Wiener diversity index:

$$H' = -\Sigma\ pi \times\ ln\ pi,$$

where pi = ni/N, pi = the proportion of the total number of individuals per species in each sample, ni = number of individuals per species, N = total number of individuals per sample (Brower et al., 1998).

Climate and river discharge time series

To test the climatic significance of the $MAR_{terr\ OM}$ and freshwater diatoms (%) preserved in Reloncaví Fjord sediments (proxies for terrestrial input), our results were compared to several instrumental and proxy time-series. More specifically, we used accumulation rates of terrestrial organic carbon and the percentage of freshwater diatoms of cores RC-6B and RC-7B, as proxies for precipitation-driven river discharge. We did not consider core RC-5B, due to the poorly-constrained chronology of this core (Table 2). The composite records were obtained from interpolating 10-yr averages in cores RC-6B and RC-7B, and then averaging the values from in each core. Our results were compared to the following instrumental and proxy time-series: i) historical precipitation at Puerto Montt (CE 1862–2010; KNMI Climate Explorer http://climexp.knmi.nl); ii) historical Puelo River discharge (CE 1948–2010; http://www.dga.cl); iii) Puelo River discharge reconstructed from tree rings (CE 1600–2000, Lara et al., 2008); iv) Fe/Al record from Quitralco Fjord (Bertrand et al., 2014a); v) the Southern Annular Mode (SAM) (from http://www.nerc-bas.ac.uk/icd/gjma/sam.html, CE 1957–2010) and the SAM-NCEP reconstructed for the CE 1409–2006 period (Villalba et al., 2012 from ftp://ftp.ncdc.noaa.gov/pub/data/paleo/treering/reconstructions/villalba2012sam.txt); and vi) alkenone-derived sea surface temperature (SST) anomaly for 41–51°S, which was obtained using four SST records: GeoB3313 (41°S; Lamy et al., 2002), GeoB7186 (44°S; Mohtadi et al., 2007), PC33 (44°S; Sepúlveda et al., 2009), and MD07-3124 (51°S; Caniupán et al., 2014). These four records were interpolated at 1-yr intervals using the Interp component of Arand software (http://www.ncdc.noaa.gov/paleo/softlib/arand/arand.html), and SST anomalies were calculated independently for each record, using the CE 1300–2000 period as a reference (Bertrand et al., 2014a). The resulting SST anomalies (deviation from the mean, in °C) were then averaged over the four cores. Other data are also expressed as anomalies (precipitation and river discharge), which were calculated by subtracting the mean from each observation and dividing them by the historic standard deviation of the respective series.

Results

Surface sediments

A clear spatial segregation pattern emerges from results of geochemical parameters in surface sediments (Table 1, Fig. 2). Higher Si_{OPAL} (7.83 ± 1.55%) and C_{org} values (1.74 ± 0.54%), lower N/C (0.08 ± 0.02) and more depleted $\delta^{13}C_{org}$ values (−24.77 ± 1.46‰) were found in sediments near the main river discharges than at the stations located closer to the fjord mouth, which displayed lower Si_{OPAL} (5.67 ± 1.27%) and C_{org} values (0.62 ± 0.54%), higher N/C (0.13 ± 0.06), and less depleted $\delta^{13}C_{org}$ values (−23.70 ± 1.12‰).

Sediment cores

Sediments of the Reloncaví Fjord were dark brown and dark olive gray in color (7.5 yr 3/2 and 5 yr 3/2 on the Munsell color scale), and composed predominantly of sandy silt with low percentage of clays

(<10%) (Fig. 3). Distinct fine sand layers of variable thickness were found in each core (Fig. 3): RC-5B (33–40 cm and 74–75 cm), RC-6B (40–45 cm and 75–76 cm), and RC-7B (76–77 cm). These layers also contained plant remains and roots. Smear-slides observation excluded the presence of angular and fragmented quartz associated with volcanic eruptions mentioned previously, probably due the eastward transport of volcanic ashes by the prevailing SWW (Bertrand et al., 2014b).

Dry bulk density values were 0.82–1.99 g cm^{-3} in core RC-5B, 0.43–1.63 g cm^{-3} in core RC-6B, and 0.16–1.15 g cm^{-3} in core RC-7B. Magnetic susceptibility fluctuated between 27 and 936 $\times 10^{-8}$ SI. In all cores, the highest DBD and magnetic susceptibility values were associated with the sand layers (Fig. 3). Average grain size fluctuated between 20 and 100 μm, except for the sand layers, which reached values of up to 600 μm. Skewness ranged between 0.5 and −2, kurtosis was 2–9, and sorting ranged 3–7. Sediments were in general mesokurtic to leptokurtic in sand layers and poorly sorted (Fig. 3).

Chronology

The age models are shown in Figure 4. We rejected two sediment samples from RC-5B that most likely are part of a reworked deposit since they are located immediately on top and below the sand layer (Fig. 4, Table 2). They could be part of a turbidite/event deposit that is thicker than the sand layer itself. Also, we discarded the marine mollusk age, because the marine reservoir age is very variable in fjords where water exchange with open ocean is limited (Olsen et al., 2009), and thus the shell fragment found may not be very reliable for dating in Reloncaví Fjord.

The ^{210}Pb activities in the three cores display a clear pattern of exponential decay. Background values of 0.56 ± 0.18, 0.40 ± 0.07 and 0.66 ± 0.04 dpm g^{-1} were recorded at 35, 22, and 20 cm depth for cores RC-5B, RC-6B and RC-7B, respectively. According to our age models cores RC-5B and RC-6B span the last 700–800 yr, and core RC-7B covers the last 300 yr. Average sedimentation rates obtained from CLAM 2.1 software were 0.18, 0.14 and 0.24 cm yr^{-1} for cores RC-5B, RC-6B, RC-7B, respectively. Variations in accumulation rates through time are presented in Figure 4.

The ages assigned to the sand layers in core RC-5B at 33–40 cm and 74–75 cm are CE 1795–1865 and CE 1070–1430 (highest probability: CE 1280–1360), respectively. In core RC-6B, ages assigned to the sand layers at 40–45 cm and 75–76 cm are CE 1600–1950 (highest probability: CE 1700–1800) and CE 1140–1350, respectively. Finally the sand layer at 76–77 cm in core RC-7B was dated at CE 1580–1740 (Fig. 4).

Geochemistry of the sediment cores

The content of Si_{OPAL} was higher, on average, in core RC-5B (8.2%) followed by core RC-7B (5.9%) and core RC-6B (5.8%) (Fig. 5a, f, k). An increase in Si_{OPAL} toward the present was evident in cores RC-6B (since ~1800) and RC-7B (most prominent since ~1900s) but not in core RC-5B, which showed values fluctuating between 6 and 11% during the last 200 yr. The content of C_{org} in all three cores oscillated between 0.02 (lowest values generally associated with the sand layers) and 2.1%.

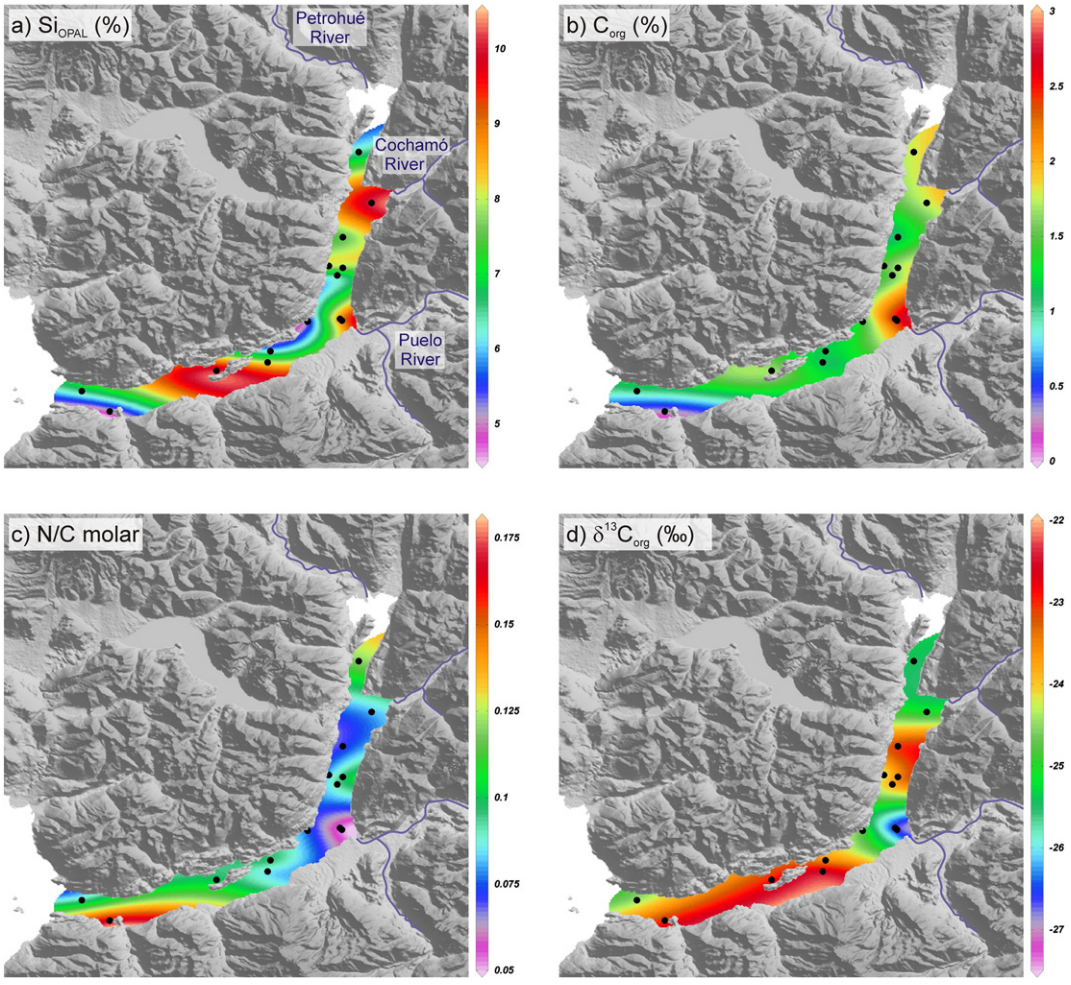

Figure 2. Geochemical characteristics in surface sediments of the Reloncaví Fjord. Graphic representation (Ocean Data View software ODV 4) of the spatial distribution of a) biogenic silica Si_{OPAL}, b) organic carbon C_{org}, c) N/C molar ratio, and d) stable carbon isotopes $\delta^{13}C_{org}$. The main rivers are indicated.

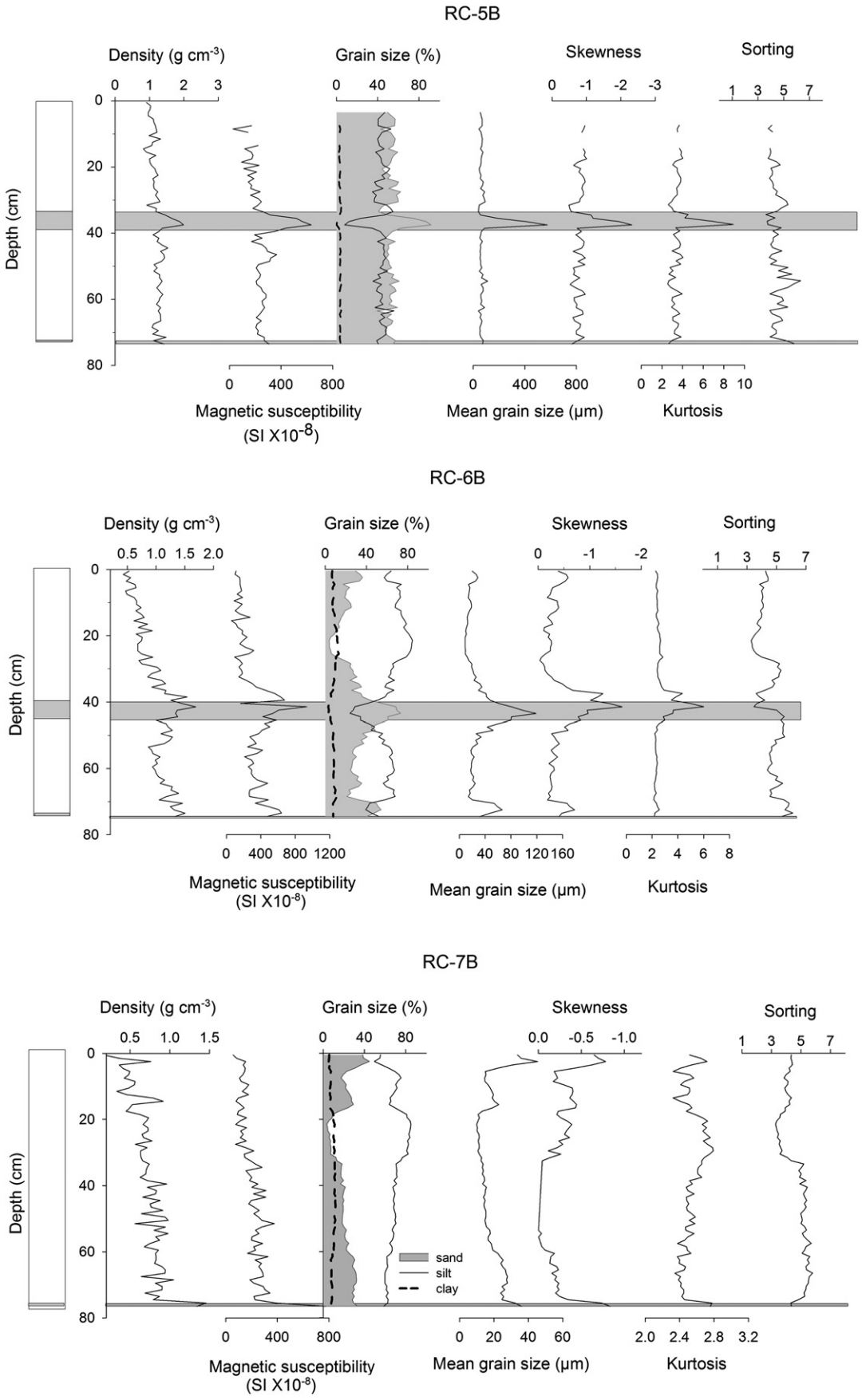

Figure 3. Sedimentological and granulometric characteristics of sediment cores RC-5B, RC-6B and RC-7B from the Reloncaví Fjord. Horizontal gray bars indicate the presence of sand layers.

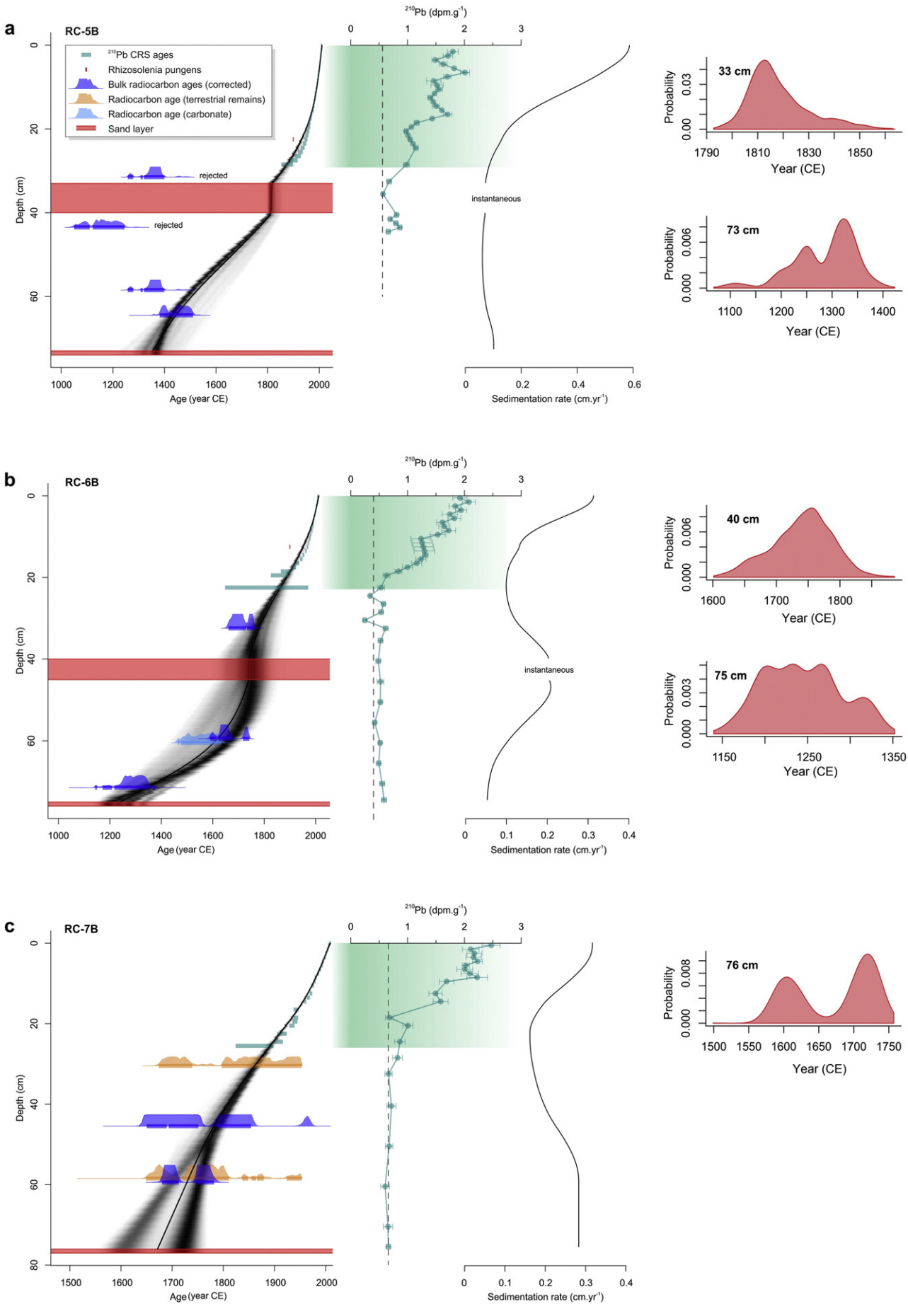
a
RC-5B
^{210}Pb CRS ages
Rhizosolenia pungens
Bulk radiocarbon ages (corrected)
Radiocarbon age (terrestrial remains)
Radiocarbon age (carbonate)
Sand layer
rejected
rejected
^{210}Pb (dpm.g^{-1})
instantaneous
Depth (cm)
Age (year CE)
Sedimentation rate (cm.yr^{-1})
33 cm
73 cm
Probability
Year (CE)
b
RC-6B
40 cm
75 cm
c
RC-7B
76 cm

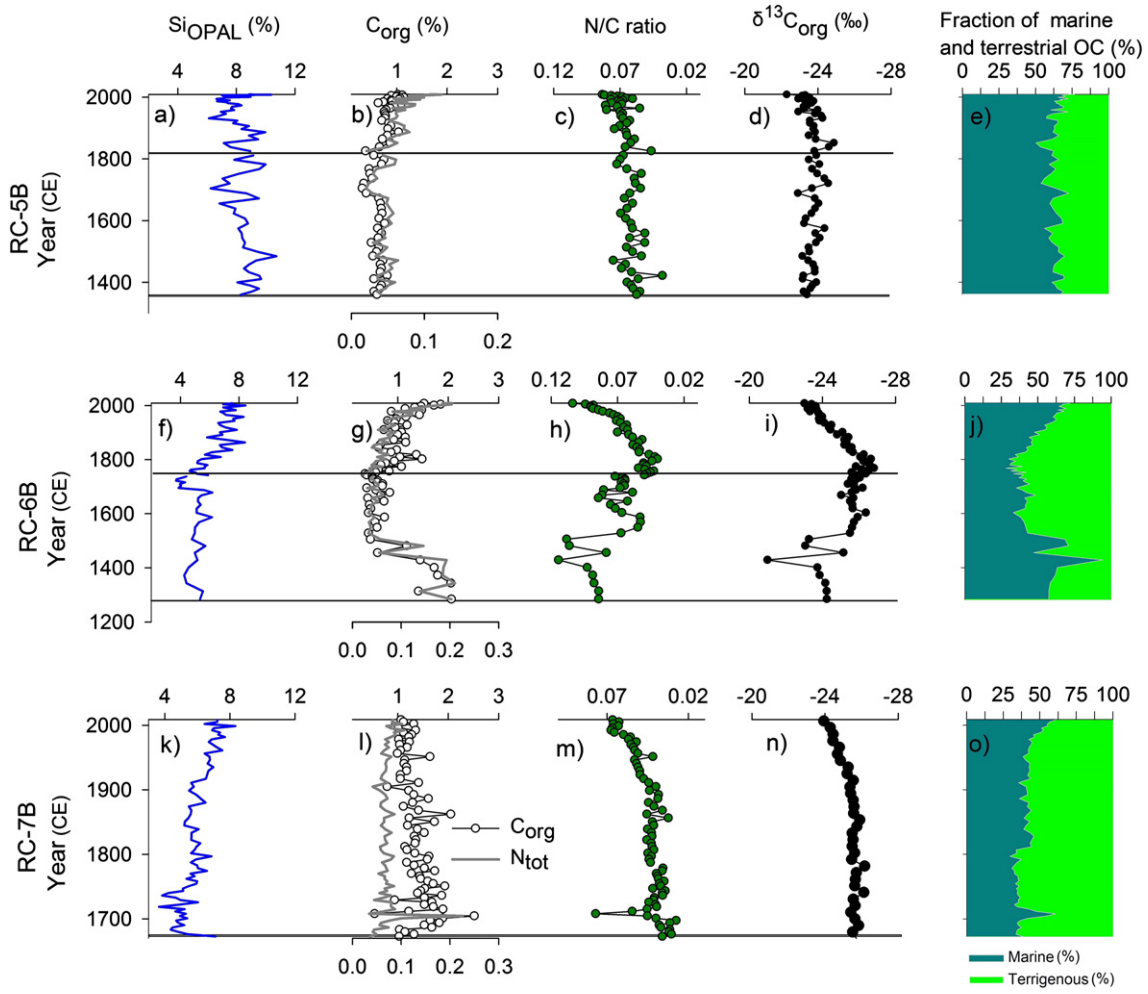

Figure 5. Reloncaví Fjord downcore geochemical characteristics plotted against age. Geochemical characteristics in cores RC-5B, RC-6B and RC-7B (biogenic silica Si_{OPAL}, organic carbon C_{org}, total nitrogen N_{tot}, N/C molar ratio, and stable carbon isotopes $\delta^{13}C_{org}$), and the proportion of terrigenous and marine OM from two-source mixing model of Thornton and McManus (1994). Horizontal gray bars indicate sand layers.

The patterns of N_{tot} were similar to those of C_{org} with values of 0.004–0.23% (Fig. 5b, g, l). In RC-5B and RC-6B, there was a strong positive correlation between C_{org} and N_{tot} (RC-5B: r Pearson = 0.94, $p < 0.05$; RC-6B: r Pearson = 0.91, $p < 0.05$) but this correlation was less robust in core RC-7B (r Pearson = 0.64, $p < 0.05$). The N/C molar ratio varied between 0.10 and ~0.03 (Fig. 5c, h, m). $\delta^{13}C_{org}$ ranged between −20.5 and −27.6‰ (with depleted values in the sand layers) that reflect a mixture of allochthonous (terrestrial) and autochtonous (marine) OM sources. $\delta^{13}C_{org}$ increased toward the present in core RC-6B, as well as (more subtly) in core RC-7B (Fig. 5d, i, n).

The results of the two-source mixing model based on $\delta^{13}C_{org}$ in the three cores showed a clear decrease in the fraction of terrestrial carbon toward the present, which was most evident in core RC-6B since CE 1800, and since the mid-1900s in core RC-7B (Fig. 5e, j,o). The average proportion of terrestrial OM in cores RC-5B, RC-6B and RC-7B amounted to 36%, 52% and 59%, respectively.

Siliceous microorganisms

Diatoms represented 98% of the total siliceous microfossil assemblage; silicoflagellates, sponge spicules, chrysophyte cyts and phytoliths were a very minor component (Fig. 6). Thus, only the diatom results are presented here. Figures 7 and 8 summarize the downcore fluctuations in Si_{OPAL}, total diatoms (valves g^{-1}), diatom diversity (Shannon index H'), and the main ecological diatom groups with their representative species for cores RC-6B and RC-7B. Si_{OPAL} and total diatoms content were positively correlated in both cores (RC 6B, $r^2 = 0.67$, $p < 0.01$; RC-7B, $r^2 = 0.62$, $p < 0.01$), indicating that for the Reloncaví Fjord, Si_{OPAL} is a good indicator of changes in diatom abundance (Figs. 7a, b; 8a, b). Diatom diversity in cores RC-6B and RC-7B varied between 1.5 and 3.5 (Figs. 7b and 8b), and along with Si_{OPAL} and diatom abundance, showed a clear decrease in the sand layers mainly in core RC-6B.

The high-nutrient group (HN), mainly represented by resting spores of the genus *Chaetoceros*, was somewhat more abundant in core RC-6B than in RC-7B; on average 48% and 41%, respectively. Spores of *Chaetoceros radicans/cinctus* contributed 22% in core RC-6B and ca. 14% in RC-7C (Figs. 7c, 8c). A decreasing trend in the contribution of this group and its main species is evident in core RC-6B since CE 1900. The coastal-planktonic group (CP) contributed with ca. 25% in both cores, with *Cyclotella litoralis* as the main species (14% in core RC 6B and ~9% in core RC 7B) (Figs. 7d, 8d). Within the CP group, the first occurrence

Figure 4. Chronologies of cores RC-5B, RC-6B and RC-7B. a–c. Age models for RC-5B, RC-6B, RC-7B based on ^{210}Pb ages, AMS-^{14}C, and the first occurrence of *Rhizosolenia setigera* f. *pungens* (abbreviated as R. *pungens*) in the downcore record. Downcore profiles of total ^{210}Pb activities; the horizontal error bars represent on standard deviation (1 s) based on the propagation of ^{210}Pb and the standard deviation of the background. The vertical dotted line is the supported activity (background) and the line represents the sedimentation rates for each core. The graphs to the right indicate the most probable age of the sand layers.

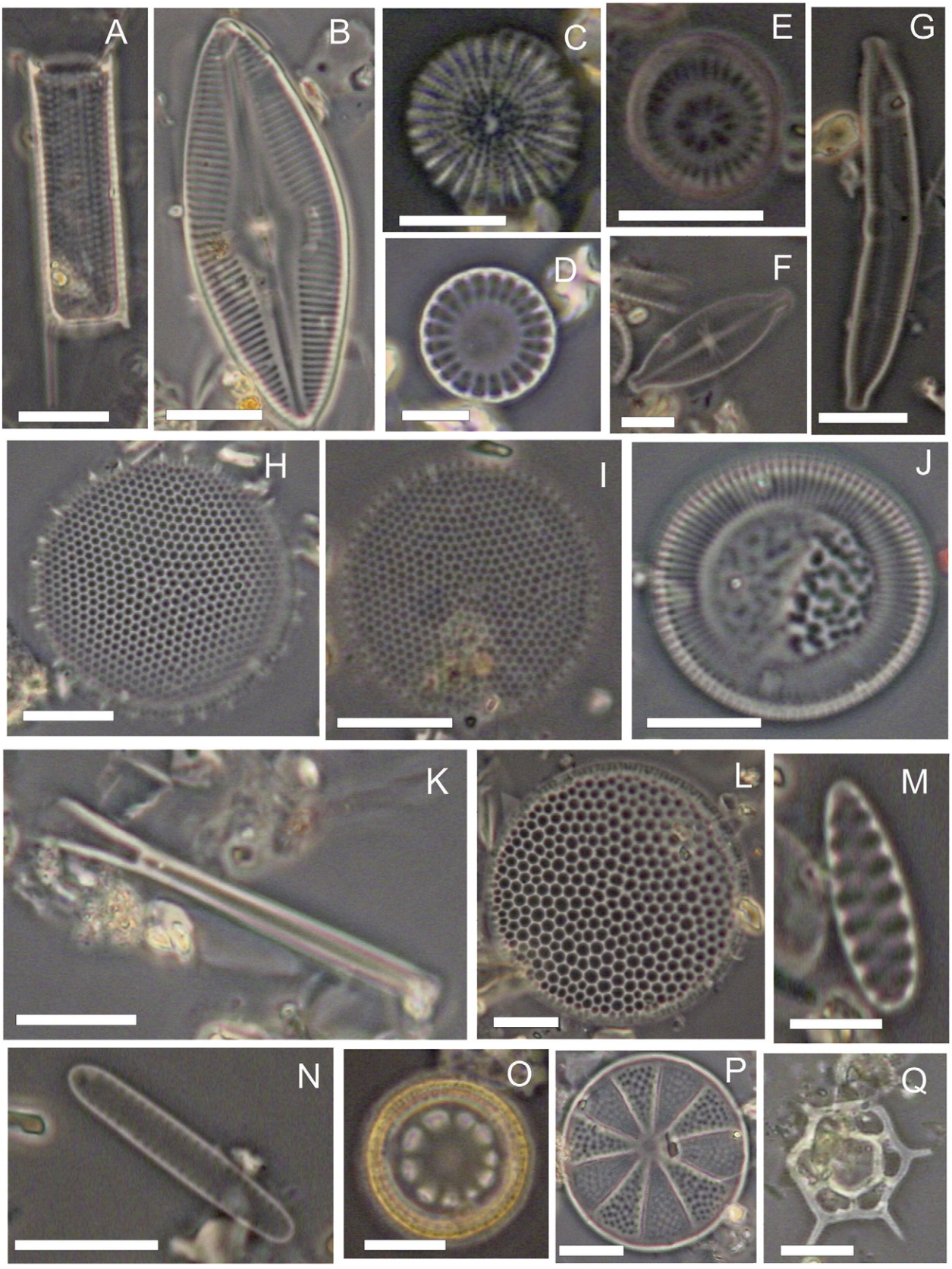

Figure 6. Siliceous microorganisms preserved in Reloncaví Fjord sediments. Most important diatoms (A–P) and the silicoflagellate *Distephanus speculum* (Q). (A) *Aulacoseira granulata*., (B) *Navicula palpebralis*, (C) *Stephanodiscus astraea*, (D) *Cyclotella meneghiniana*, (E) *Discostella stelligera*, (F) *Navicula decussis*, (G) *Hannaea arcus*, (H) *Thalassiosira eccentrica*, (I) *Thalassiosira pacifica*, (J) *Cyclotella litoralis*, (K) process of *Rhizosolenia setigera* f. *pungens*, (L) *Coscinodiscusradiatus/marginatus*, (M) *Opephora pacifica*, (N) *Thalassionema nitzschioides* var. *nitzschioides*, (O) *Paralia sulcata*, and (P) *Actinoptychus vulgaris*. Scale = 10 μm in Figs. A, B, G–L, and N–Q. Scale = 5 μm in Figs. C–F and M.

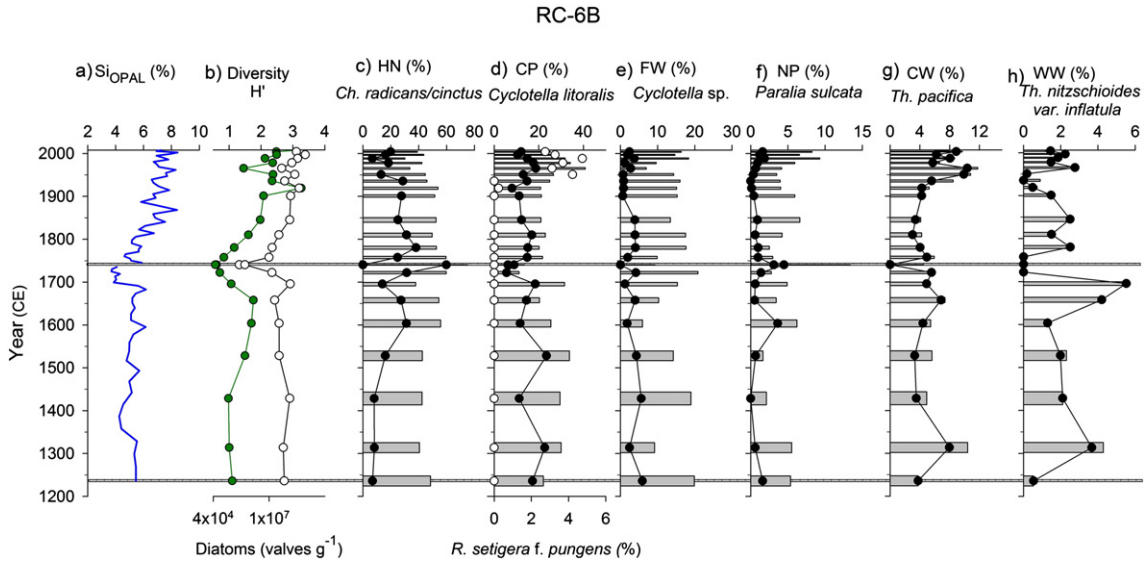

Figure 7. Biogenic opal and diatoms of Core RC-6B, Reloncaví Fjord. a) Si_{OPAL} content (%);b) total diatoms (valves g^{-1}, green circles) and Shannon–Wiener diversity index (*H'*, white circles); and c–h) main ecological diatom groups high nutrient (HN), coastal planktonic (CP), non-planktonic (NP), freshwater (FW), warm water (WW), and cold water (CW). White circles in the CP group mark the occurrence of *Rhisozolenia setigera* f. *pungens*; note that the first appearance in this record is ~CE 1919. Gray horizontal bars show the two sand layers in this core (see also Fig. 4).

of *R. setigera* f. *pungens* in the downcore records is noteworthy: from 16–17 cm (RC-6B) and 32–33 cm (RC-7B) onwards, corresponding to an age of CE 1902 ± 25 in both cores. The freshwater group (FW) contributed on average 14% (RC-6B) and ~17% (RC-7B) of the total assemblage; *Cyclotella* spp. was the most important genus (3%), followed by *Aulacoseira granulata* (2%) and minor contributions of *Rhoiscophenia curvata*, *Navicula decussis*, *Cyclotella meneghiniana*, *Hannaea arcus* (Figs. 7e, 8e). The non-planktonic group (NP), represented by *Paralia sulcata*, *Opehora pacifica* and *Diploneis subovalis* as characteristic species, contributed with 6% to the total assemblage. Greater representation of *P. sulcata* was observed mainly in the sand layer at 44–45 cm in core RC-6B (Fig. 7f). On average, the cold water group (CW) contributed ~6% in both cores, with *Thalassiosira pacifica* being the most abundant species (Figs. 7g, 8g). Finally, the least abundant group was the warm water group (WW) which averaged ~0.2 and 2% in cores RC-6B and RC-7B, respectively (Figs. 7h, 8h); *Thalassionema nitzschioides* var. *inflatula* characterized this assemblage.

Discussion

Surface sediments in Reloncaví Fjord

Si_{OPAL} in the Reloncaví Fjord ranged 4–10.5%, which is in agreement with those values reported by Aracena et al. (2011) and Bertrand et al. (2012a) for Northern Patagonia fjords (1.8–17.7%). The high abundance of diatoms and the positive correlation of Si_{OPAL} with total diatom concentrations demonstrate that this siliceous group dominates the biogenic silica signal in Reloncaví Fjord sediments, in agreement with previous studies (Rebolledo et al., 2005; Sepúlveda et al., 2005; Mayr et al., 2014).

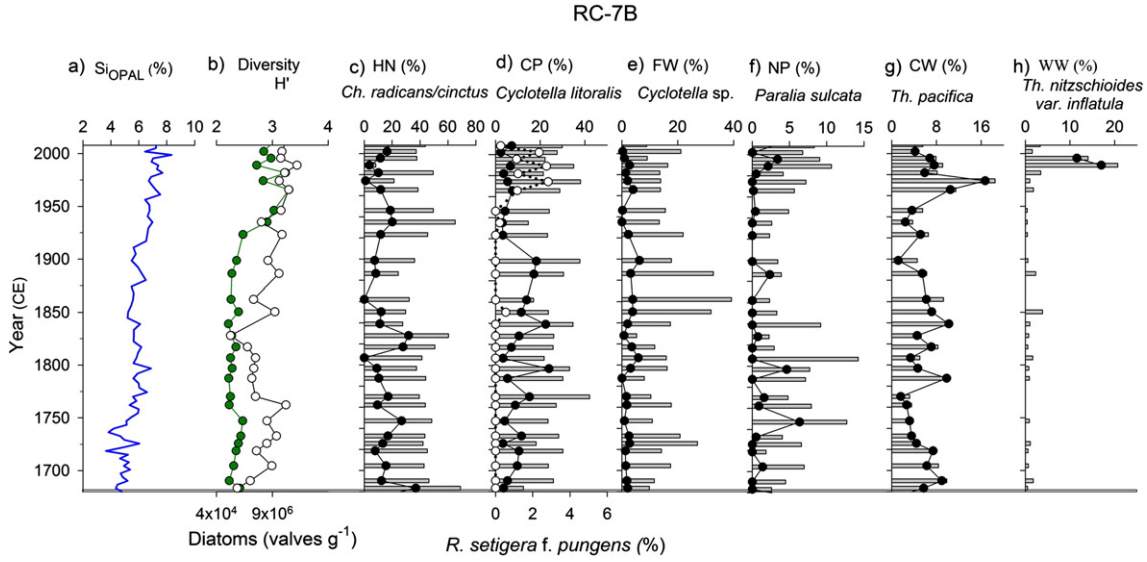

Figure 8. Biogenic opal and diatoms of Core RC-7B, Reloncaví Fjord. a) Si_{OPAL} content (%); b) total diatoms (valves g^{-1}, green circles) and Shannon–Wiener diversity index (*H'*, white circles); and c–h) main ecological diatom groups high nutrient (HN), coastal planktonic (CP), non-planktonic (NP), freshwater (FW), warm water (WW), and cold water (CW). White circles in the CP group mark the occurrence of *Rhisozolenia setigera* f. *pungens*; note that the first appearance in this record is ~ CE 1884. Gray horizontal bars show the two sand layers in this core (see also Fig. 4).

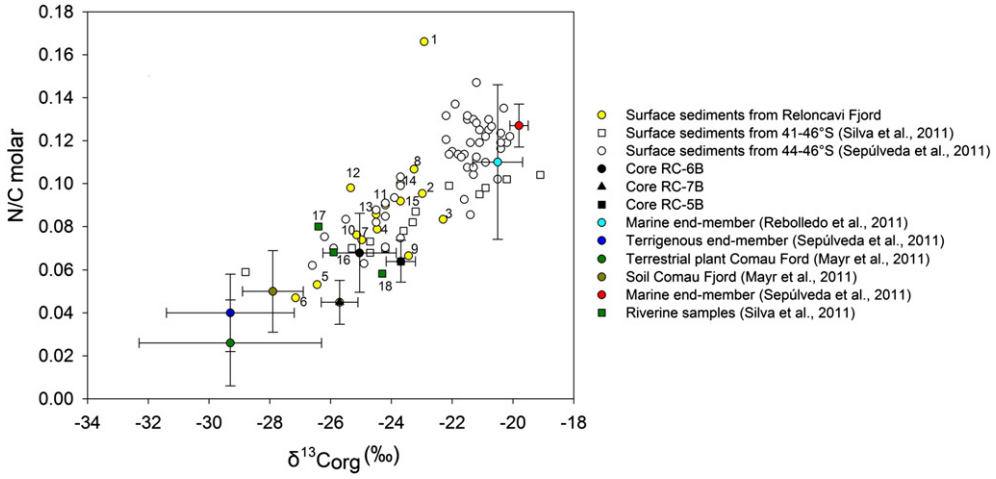

Figure 9. Compilation plot of N/C molar ratio vs. $\delta^{13}C_{org}$ for surface sediments and downcore records in the Reloncaví Fjord (for locations see Table 1, the number represents the locations for each sample). Surface sediments from 41–46°S given by Silva et al. (2011), and surface sediments from 44–46°S reported by Sepúlveda et al. (2011). Marine end-member from Rebolledo et al. (2011) refers to the downcore average value of core MD07-3109H from the Ancud Gulf (42°S, 72°W). Marine end-member from Sepúlveda et al. (2011) was obtained by averaging values from outside the fjord area in the Boca del Guafo with values from continental slope sediments from Hebbeln et al. (2000). Terrestrial end-member is adopted from Sepúlveda et al. (2011) based on river sediments and degraded and fresh plant material in Northern Patagonia, and on soil samples and plants from Mayr et al. (2011). Error bars = standard deviation.

C_{org} values in fjord sediments ranged mostly between 0.5 and ~3%, whereas higher values were observed in riverine sediment samples (Puelo River C10F-51: 3.6%; Petrohué River C10F-53: 9.3%; Table 1). Contents in Reloncaví Fjord fall within the range of those reported for the Inner Sea of Chiloé and other Northern Patagonia fjords (0.5–4%; see review in Aracena et al., 2011; Bertrand et al., 2012c).

Sources of organic matter in the Reloncaví Fjord

In order to place the bulk organic geochemical results obtained on Reloncaví surface and downcore sediments in a regional context, we used i) available information on N/C molar ratio and $\delta^{13}C_{org}$ for Northern Patagonia fjords (41–46° S; Sepúlveda et al., 2011; Silva et al., 2011); ii) the marine end-member values for N/C molar ratio and $\delta^{13}C_{org}$ from Rebolledo et al. (2011) and Sepúlveda et al. (2011); iii) the terrigenous end-member values from Sepúlveda et al. (2011); and iv) the soil and terrestrial values from Comau Fjord at 42°S (Mayr et al., 2011). When plotting the N/C molar ratio and $\delta^{13}C_{org}$ for the surface sediments jointly with the downcore average values for cores RC-5B, RC-6B and RC-7B (Fig. 9) it is evident that the organic matter of all our Reloncaví Fjord sediment samples (surface and downcore) is composed of a mixture of the two marine and terrestrial sources, in variable proportions. The values of N/C molar ratio (0.04–0.17) and $\delta^{13}C_{org}$ (from −22 to −27‰) follow a spatial pattern that reflects the origin of the OM, where the stations nearest to river inflows exhibit lower N/C and depleted $\delta^{13}C_{org}$ values. Furthermore, the average downcore value of core RC-7B is plotting near the values of the terrestrial end-member (e.g., soil values from the Comau Fjord; 42°S; Mayr et al., 2011) (Fig. 9), reflecting the high input of terrestrial organic matter in this inner fjord sediment core. Overall, averaging all N/C and $\delta^{13}C_{org}$ values for surface and downcore sediments, we obtain values of N/C = 0.079 ± 0.027 and $\delta^{13}C_{org}$ = −24.49 ± 1.27 thus reflecting the important contribution of terrigenous OM in the Reloncaví Fjord.

Diatom assemblages in sediments as recorders of seasonal fluctuations in the water column and statigraphic markers

In the Inner Sea of Chiloé, González et al. (2010) have shown that the higher radiation and enhanced photoperiod of spring together with the continuous supply of freshwater loaded with silicic acid promote the growth of chain-forming diatoms >20 μm in the water column. The genera *Chaetoceros*, *Skeletonema* and *Thalassiosira* dominate the spring microphytoplankton in Northern Patagonia (Iriarte et al., 2007; González et al., 2010). Highest abundances of *Rhizosolenia* spp. occur in spring and summer, and are associated with a more stratified water column (Alves-de-Souza et al., 2008; Iriarte et al., 2010).

In our sediment cores RC-6B and RC-7B, the diatom genus *Chaetoceros* was represented by abundant resting spores (>40% of the diatom assemblage; Figs. 7c and 8c), whereas the genera *Skeletonema* spp., *Thalassiosira* (*T. eccentrica*, *T. oestrupii*, *T. angulata*, *T. tenera*) and the species *Rhizosolenia setigera* f. *pungens* were common members of the sediment assemblage but never abundant and represented on average 3%, 6% and 2% of the total diatom assemblage, respectively. Thus, we infer that only part of the spring–summer diatom signal is actually preserved in the sediments of the Reloncaví Fjord.

The euryhaline diatom *R. setigera* f. *pungens* (Sancetta et al., 1991) is present in cores RC-6B and RC-7B from ~CE 1902 ± 25 onwards which agrees with other sedimentary studies from Northern Patagonia, and confirms its first occurrence as a robust geochronological marker (Rebolledo et al., 2011). In the area of the Reloncaví Sound, the first

Figure 10. Compilation of sedimentological proxies preserved in Reloncaví Fjord sediments, and historical and reconstructed climatological time-series. a) Composite of terrigenous mass accumulation rate ($MAR_{terr\ OM}$, green line) obtained from interpolating 10-year averages of $MAR_{terr\ OM}$ in cores RC-6B and RC-7B, and composite freshwater diatoms (%, blue line) from cores RC-6B and RC-7B obtained in the same way as $MAR_{terr\ OM}$. b) Historical record of precipitation at Puerto Montt (blue line; CE 1862–2010; http://climexp.knmi.nl) plotted together with instrumental record of Puelo River discharge (light blue line; CE 1957–2010, http://www. dga.cl), and reconstructed Puelo River discharge from Lara et al. (2008), gray line (CE 1600–2000). c) Fe/Al (g/g) in Quitralco fjord at 46°S (red circles; Bertrand et al., 2014a). d) Periods of high precipitation in Lago Puyehue at 41°S (dark-yellow rectangle; Bertrand et al., 2005), in the Jacaf Fjord at 44°S (green rectangles; Sepúlveda et al., 2009), and Lago Plomo 47°S (winter precipitation only; yellow rectangles; Elbert et al., 2011). e) Southern Annular Mode (SAM), black line (1957–2010; from http://www.nerc-bas.ac.uk/icd/gjma/sam.html), and reconstructed SAM-NCEP index from Villalba et al. (2012;ftp://ftp.ncdc.noaa.gov/pub/data/paleo/treering/reconstructions/villalba2012sam.txt), gray line. Black lines in b and c, and red line in c indicate two-year running average. f) Composite alkenone-derived SST anomaly based on available records off Chilean Patagonia (41–51°S; GeoB3313 (41°S; Lamy et al., 2002), GeoB7186 (44°S; Mohtadi et al., 2007), PC33 (44°S; Sepúlveda et al., 2009), and MD07-3124 (51°S; Caniupán et al., 2014); red line indicates average SST anomaly and the gray envelope represents the standard deviation (Bertrand et al., 2014a). Vertical gray rectangles highlight the highest precipitation seasonality periods.

occurrence of *R. setigera* f. *pungens* in the sedimentary record (Rebolledo et al., 2011) coincides with the construction of the Puerto Montt pier in ~CE 1888 and later installation of the port of Puerto Montt (http://www.empormontt.cl/sitio/es/historia), raising the possibility that this species has been introduced to the area by ships' ballast water.

Downcore diatom concentrations average 8×10^6 valves g^{-1} for core RC-6B and 5×10^6 valves g^{-1} for core RC-7B, excluding sand layers. These values are one order of magnitude lower than those recorded in other Northern Patagonia fjords (i.e., Puyuhuapi, Jacaf and Comau, all with ca. 10^7 valves g^{-1}; Rebolledo et al., 2005, 2008; Mayr et al.,

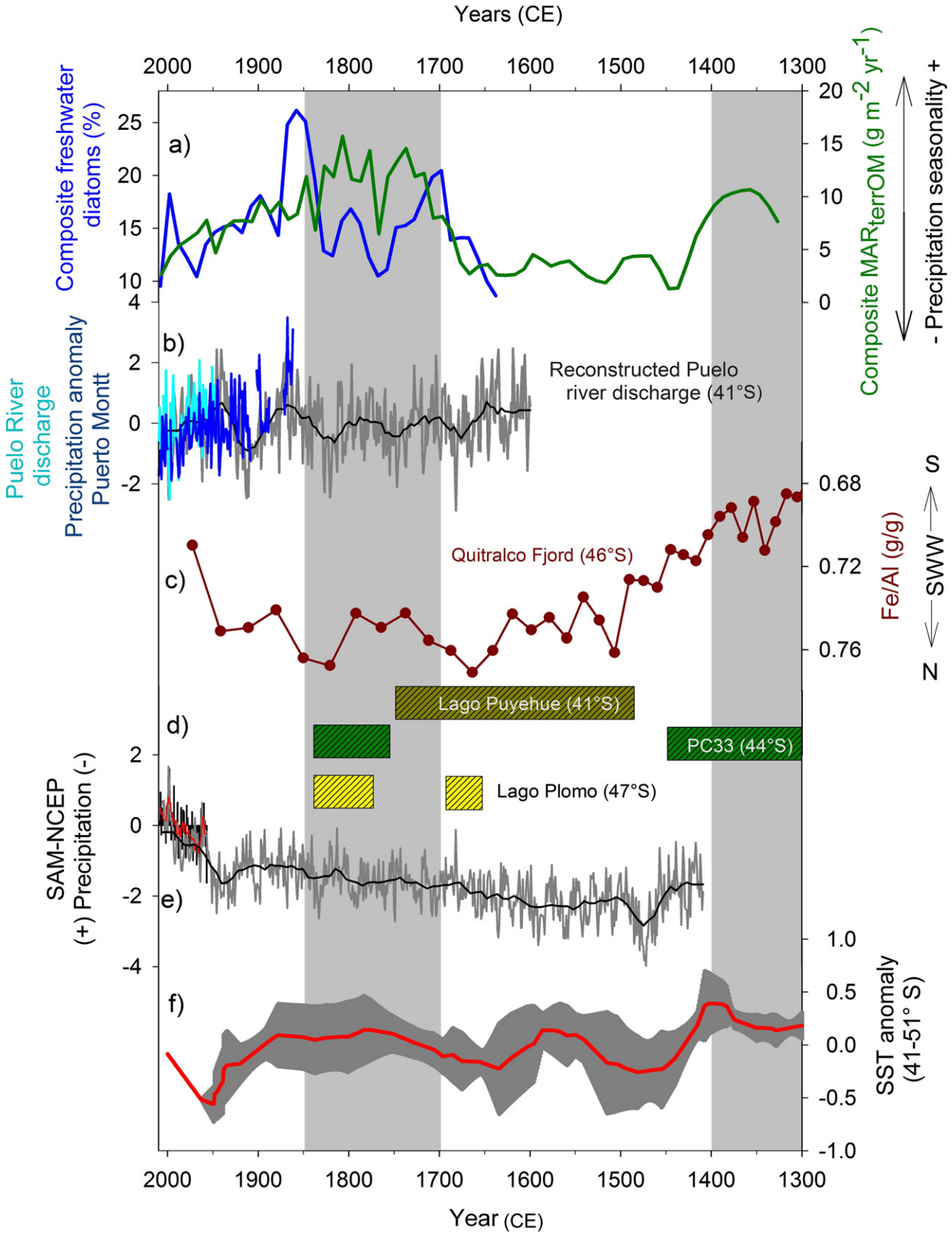

2014), possibly due to dilution by high terrestrial input that characterizes the Reloncaví Fjord.

Sand layers in cores RC-6B and RC-7B were characterized by lowest diatom abundances, low diversity, and an increment in the contribution of *Paralia sulcata* within the NP group (from 1% outside the sand layer to 4% inside, core RC-6B). This species has been described as an indicator of high energy environments in Swedish fjords (McQuoid and Nordberg, 2003) and its higher contribution in sand layers of West Point, Washington, has been associated with paleo-tsunami events (Hemphill-Haley, 1996).

The possible origin of sand layers in Reloncaví Fjord sediments

Based on geochronological, geochemical analysis and historical evidences, we believe that the sand layers described in sediment cores RC-5B, RC-6B and RC-7B represent remobilized sediments during the large earthquakes that affected the area in the last millennium (e.g., Cisternas et al., 2005). They likely represent coarse material supplied by subaquatic and aerial (landslide) slope failures, resembling what occurred in Aysén fjord during the 2007 M_w 6.2earthquake (Naranjo et al., 2009; Van Daele et al., 2013). Moreover, the increase in the diatom *Paralia sulcata* in sand layers seems to be associated with landslides triggered by earthquakes. Because sand layers in our cores have a terrestrial origin (with depleted δ^{13}Corg and low N/C values; Fig. 5) we cannot assume a tsunamigenic origin. Diatoms have been widely used as indicators of coseismic subsidence and uplift associated with earthquakes events in coastal sediments and buried soils (Cisternas et al., 2005; Horton et al., 2011; Garret et al., 2013).

According to our age models (Fig. 4), the upper sand layers in cores RC-5B (33–40 cm) and RC-6B (40–45 cm) most likely represent the CE 1737 or CE 1837 earthquakes, which were clearly described in historical documents but not recorded in the sediments of the nearby Maullín estuary (Cisternas et al., 2005). Cores RC-5B and RC-6B do not seem to have recorded the large CE 1575 earthquake that affected the region (Cisternas et al., 2005; St-Onge et al, 2012). The single sand layer described in core RC-7B could correspond to either the CE 1575 or CE 1737 earthquake.

By comparison, St-Onge et al. (2012) found no evidence of sand layers associated with the CE 1837 and CE 1737 earthquakes in sediment core MD07-3108Cq, which was taken at the mouth of the Reloncaví Fjord. They however did find tsunami sand layers related to the CE 1960 and CE 1575 earthquakes. Seismic profiles from the head and middle of the fjord provided additional evidence for mass wasting deposits associated with the earthquake of CE 1960, CE 1575 and ~CE 1200–1400. A turbidite was recorded in a sediment core recovered near Puelo River (RC-5C; 41°38′S, 72° 20′ W), in the middle part of the fjord (Fig. 1a). In this core, Marín (2014) described a sand layer at 25–14 cm, which was dated at CE 1964 ± 4, characterized by low values of $^{210}Pb_{excess}$, Si_{OPAL} and by an increase in sand percentages. Within age uncertainties, it could be a recorder of either the CE 1960 earthquake or the historical landslide-debris flow deposit of CE 1965 from the adjacent Yate volcano (Fig. 1; Watt et al., 2009; Marín, 2014; Rebolledo et al., 2014). This suggests that the earthquake-triggered turbidites associated with the CE 1960 M_W 9.5 subduction earthquake were mainly restricted to the outer part of the fjords (St-Onge et al., 2012).

The deeper sand layers in cores RC-5B (74–75 cm) and RC-6B (75–76 cm) may correspond to pre-historical seismic activity in the fourteen and fifteen centuries, as described by Cisternas et al. (2005), possibly the CE 1319 earthquake (Moernaut et al., 2014). We do not have enough data to make any links to these older events.

Variations in OM sources and relation to climate variability

In Chilean Patagonia, precipitation is linked to the SWW. Multidecadal variability in the strength and latitudinal movements of the SWW belt has been associated with the SAM, a measure of the pressure gradient between Southern Hemisphere mid-and high latitudes and the El Niño-Southern Oscillation (ENSO) (Garreaud et al., 2009; Quintana and Aceituno, 2012; Villalba et al., 2012; Moreno et al., 2014).

Organic matter of terrigenous origin and the contents of freshwater diatoms in sediments have been used as proxies of changes in precipitation on land and river discharge into Patagonian fjord environments (e.g., Rebolledo et al., 2005, 2011; Sepúlveda et al., 2009; Mayr et al., 2014). Here, we assessed the use of $MAR_{terr\ OM}$ and freshwater diatoms (%) in Reloncaví Fjord as proxies for temporal changes in terrigenous input related to precipitation and river discharge. The correlation between monthly precipitation at Puerto Montt and Puelo River discharge (for CE 1948 − 2010) was high and positive (r Pearson = 0.68, $p < 0.05$). Thus, for the last ~700 yr, we use composite $MAR_{terr\ OM}$ (CE 1328 − 2010) and composite freshwater diatoms (%) (CE 1688 − 2010) in cores RC-6B and RC-7B (discarding turbidite intervals; for more details, see section Material and methods) (Fig. 10a), and compare our two proxy records with instrumental and reconstructed time series of precipitation and Puelo River discharge (Fig. 10b) and Fe/Al record from Quitralco Fjord (Bertrand et al., 2014a) (Fig. 10c), proxy records of SAM (Fig. 10e), and SST for 41–51°S (Fig. 10f) (see Material and methods section for details). We observe increased $MAR_{terr\ OM}$ in CE 1300–1400 and CE 1700–1850, when in Quitralco Fjord (Bertrand et al., 2014a) precipitation seasonality is high (higher during CE 1300–1400 than during CE 1700–1800). Our interpretation is that in both Reloncaví and Quitralco, precipitation seasonality also controls terrestrial erosion, which is recorded in terrestrial OM accumulation rates. This is in agreement with the record of Bertrand et al. (2005) for Lago Puyehue (41°S), who interpreted increased accumulation rates of terrigenous particles in the lake as a result of higher river discharge due to increased precipitation. Also, Sepúlveda et al. (2009) using a multi-proxy approach in a core recovered from the Jacaf Fjord (44° S), suggested higher precipitation between CE 1200 and 1450 and during CE 1750–1850. A recent precipitation reconstruction from Lago Plomo (47°S, Elbert et al., 2011) shows wet phases at ca. CE 1600, CE 1630–1690, and CE 1780–1850 (Fig. 10d). Based on these comparison, we infer that the highest precipitation seasonality recorded in Reloncaví Fjord sediments in CE 1700–1850 (and probably also between CE 1300 and 1400) is coeval with positive anomaly SSTs in Patagonia (Fig. 10).

For the last ~150 yr, $MAR_{terr\ OM}$, freshwater diatoms and Puelo River discharge reveal a decreasing trend toward the present (Fig. 10a, b). This is accompanied by an increasing SAM-NCEP index as well as decreasing SSTs, which accelerated since the ~1950s (Fig. 10e, f). The SAM-NCEP index reveals a long-term trend of negative values that stretch almost the entire ~600-yr series (Villalba et al., 2012), with more pronounced negative values (indicating more precipitation) during CE 1460–1635, around CE 1750, CE 1830, CE 1870, CE 1900, and CE 1925–1950 (Fig. 10e). In the last decades have been observed an ozone depletion in the stratosphere at high latitudes in the SH, and westerly flow has mostly decreased over Northern and Central Patagonia causing a drying trend to the west of the Andes (Garreaud et al., 2013). The decrease in precipitation and river discharges (Aravena and Luckman, 2008; Lara et al., 2008; León-Muñoz et al., 2013) as well as the positive phase of the SAM index have been related to a shift to higher latitudes of the SWW and associated storm tracks, to a poleward migration of the descending branch of the Hadley cell, and the consequent southern expansion of the dry subtropical belts (Shindell and Schmidt, 2004; Villalba et al., 2012; Garreaud et al., 2013) (Fig. 10).

Conclusions

Geochemical parameters (Si_{OPAL}, C_{org}, N/C, $\delta^{13}C_{org}$) in surface sediments of the Reloncaví Fjord reveal a spatial gradient of allochthonous and autochtonous organic matter with a clear terrigenous signal near the mouths of major rivers (Puelo, Cochamó and Petrohué).

Diatoms dominate the siliceous assemblages preserved in the sediments with an average value of 98%. Freshwater diatoms in Reloncaví

Fjord sediments are a good proxy of changes in precipitation over Northern Patagonia and Puelo River discharge.

Downcore records show evidence of earthquakes that affected the Reloncaví area: turbidites (sand layers), possibly associated with the historical earthquakes of CE 1837, 1737, 1575, 1200–1400. Sand layers were characterized by overall low abundance of diatoms and slight increased contribution of the species *Paralia sulcata*, an indicator of high-energy environments.

Most importantly, the sediment records show marked fluctuations in allochtonous vs. autochthonous sources of organic matter during the past 700 yr. By comparing sediment proxies with instrumental records, we showed that freshwater diatom concentrations and the $MAR_{terr\ OM}$ in Reloncaví Fjord sediments can be used as proxies for precipitation-driven river discharge. The combined increase in both variables suggests high precipitation seasonality in the Reloncaví Fjord during CE 1300–1400 and CE 1700–1850, and a clear decreasing pattern since CE 1850. $MAR_{terr\ OM}$ and freshwater diatoms match the instrumental record of rainfall available for the last 100 yr and reinforce the idea that this multi-proxy approach in Reloncaví Fjord sediments is suitable for revealing changes in climate that occurred in Northern Chilean Patagonia during the late Holocene.

Acknowledgments

This study was funded by FONDECYT #11110103 and partially by the COPAS Sur-Austral Program (PFB-31). We thank Úrsula Cifuentes (University of Concepción) for the bathymetry data of Reloncaví Fjord, Ricardo Villalba (Departamento de Dendrocronología e Historia Ambiental IANIGLA, CONICET) for the SAM-NCEP reconstructed index, and Roberto Urrutia (EULA Center, University of Concepción) for the use of the Bartington susceptibility meter. We thank the captain and crew of the L/C Tirana and RV Jürgen Winter for their valuable help during sample collection. CL and SP acknowledge support from the Hanse-Wissenschaftskolleg in Delmenhorst (Germany).

References

Acha, E.M., Mianzan, H.W., Guerrero, R., Favero, M., Bava, J., 2004. Marine fronts at the continental shelve of austral South America physical and ecological processes. Journal of Marine Systems 44 (1-2), 83–105.

Adriasola, A.C., Stöckhert, B., 2008. Cooling histories and deformation of plutonic rocks along the Liquiñe-Ofqui Fault Zone at the Los Lagos Region of Chile, 41°–42°15′S. Revista Geologica de Chile 35, 39–61.

Alves-de-Souza, C., González, M., Iriarte, J.L., 2008. Functional groups in marine phytoplankton assemblage dominated by diatoms in fjords of southern Chile. Journal of Plankton Research 30 (11), 1233–1243.

Appleby, P.G., Oldfield, F., 1978. The calculation of lead–210 dates assuming a constant rate supply of unsupported 210Pb to the sediment. Catena 5, 1–8.

Aracena, C., Lange, C.B., Iriarte, J.L., Rebolledo, L., Pantoja, S., 2011. Latitudinal patterns of export production recorded in surface sediments of the Chilean Patagonian fjord (41–55°S) as response to water column productivity. Continental Shelf Research 31, 340–355.

Aravena, J.C., Luckman, B.H., 2008. Spatio-temporal rainfall patterns in southern South America. International Journal of Climatology http://dx.doi.org/10.1002/JOC.1761.

Araya-Vergara, J.F., Viera, R., Suárez, R., 2008. El sistema submarino Reloncaví (Norpatagonia): Análisis morfoacústico, Batimetría y manto sedimentario reciente. Ciencia y Tecnología del Mar 31 (2), 5–27.

Bertrand, S., Fagel, N., 2008. Nature, origin, transport and deposition of andosol parent material in south-central Chile (36–42°S). Catena 73 (1), 10–22.

Bertrand, S., Boës, X., Castiaux, J., Charlet, F., Urrutia, R., Espinoza, C., Lepoint, G., Charlier, B., Fagel, N., 2005. Temporal evolution of sediment supply in Lago Puyenue (Southern Chile) during the last 600 yr and its climatic significance. Quaternary Research 64 (2), 163–175.

Bertrand, S., Hughen, K., Sepúlveda, J., Pantoja, S., 2012a. Geochemistry of surface sediments from the fjords of Northern Chilean Patagonia (44–47°S): spatial variability and implications for paleoclimate reconstructions. Geochimica et Cosmochimica Acta 76 (1), 125–146.

Bertrand, S., Araneda, A., Vargas, P., Jara, P., Fagel, N., Urrutia, R., 2012b. Using the N/C ratio to correct bulk radiocarbon ages from lake sediments: insights from Chilean Patagonia. Quaternary Geochronology 12, 23–29.

Bertrand, S., Hughen, K.A., Lamy, F., Stuut, J.B., Torrejón, F., Lange, C.B., 2012c. Precipitations the main driver of Neoglacial fluctuations of Gualas Glacier, Northern Patagonian Icefield. Climate of the Past 8, 519–534.

Bertrand, S., Hughen, K., Sepúlveda, J., Pantoja, S., 2014a. Late Holocene covariability of the southern westerlies and sea surface temperature in northern Chilean Patagonia. Quaternary Science Reviews 105, 195–208.

Bertrand, S., Daga, R., Bedert, R., Fontijn, K., 2014b. Deposition of the 2011–2012 Cordón Caulle tephra (Chile, 40° S) in lake sediments: implications for tephrochronology and volcanology. Journal of Geophysical Research, Earth Surface 119, 2555–2573.

Blaauw, M., 2010. Methods and code for "classical" age-modelling of radiocarbon sequences. Quaternary Geochronology 5, 512–518.

Bloesch, J., Evans, R.D., 1982. Lead–210 dating of sediments compared with accumulation rates estimated by natural markers and measured with sediment traps. Hydrobiologia 92, 579–587.

Blott, S.J., Pye, K., 2001. Gradistat: a grain size distributions and statistics package for the analysis of unconsolidated sediments. Earth Surface Processes and Landforms 26, 1233–1248.

Brower, J.E., Zar, J.H., Von Ende, C.N., 1998. Field and Laboratory Methods for General Ecology. McGraw-Hill, Dubuque, Iowa, USA (194 pp.).

Caniupán, M., Lamy, F., Lange, C.B., Kaiser, J., Kilian, R., Arz, H.W., León, T., Mollenhauer, G., Sandoval, S., De Pol-Holz, R., Pantoja, S., Wellner, J., Tidemann, R., 2014. Holocene sea surface temperature variability in the Chilean fjord. Quaternary Research 82 (2), 342–353.

Castillo, M.I., Pizarro, O., Cifuentes, U., Ramirez, N., Djurfeldt, L., 2012. Subtidal dynamics in a deep Fjord of southern Chile. Continental Shelf Research 49, 73–89.

Cembrano, J., Lara, L., 2009. The link between volcanism and tectonics in the southern volcanic zone of the Chilean Andes: a review. Tectonophysics 471, 96–113. http://dx.doi.org/10.1016/j.tecto.2009.02.038.

Chapron, E., Ariztegui, D., Mulsow, S., Villarosa, G., Pino, M., Outes, V., Juviginé, E., Crivelli, E., 2006. Impact of 1960 major subduction earthquake in Northern Patagonia (Chile, Argentina). Quaternary International 158, 58–71.

Cisternas, M., Atwater, B., Torrejón, F., Sawai, Y., Machuca, G., Lagos, M., Eipert, A., Youlton, C., Salgado, I., Kamataki, T., Shishikura, M., Rajendran, C.P., Malik, J., Rizal, Y., Husni, M., 2005. Predecessors of the giant 1960 Chile earthquake. Nature 437, 404–407.

Cochran, J.K., Frignani, M., Salamanca, M., Belluci, L.G., Guerzoni, S., 1998. Lead–210 as a tracer of atmospheric input of heavy metals in the northern Venice Lagoon. Marine Chemistry 62, 15–29.

Cupp, E.E., 1943. Marine plankton diatoms of the west coast of North America. Bulletin of the Scripps Institution of Oceanography 5, 1–238.

Elbert, J., Grosjean, M., von Gunten, L., Urrutia, R., Fisher, P., Waternburg, R., Ariztegui, D., Fujak, M., Hamann, Y., 2011. Quantitative high-resolution winter (JJA) precipitation reconstruction from varved sediments of Lago Plomo 47°S Patagonian Andes, AD 1530–2002. The Holocene 22 (4), 465–474.

Fletcher, M.S., Moreno, P.I., 2012. Vegetation, climate and fire regime changes in the Andean region of the southern Chile (38° S) covaried with centennial-scale climate anomalies in the tropical Pacific over the last 1500 years. Quaternary Science Reviews 46, 46–56.

Fontijn, M., Lachowycz, S.M., Rawson, H., Pyle, D.M., Mather, T.A., Naranjo, J.A., Moreno-Roa, H., 2014. Late Quaternary tephrostratigraphy of southern Chile and Argentina. Quaternary Science Reviews 89, 70–84.

Garreaud, R.D., Vuille, M., Compagnucci, R., Marengo, J., 2009. Present-day South American Climate. Palaeogeography, Palaeoclimatology, Palaeoecology 180–195.

Garreaud, R.D., Lopez, P., Minvielle, M., Rojas, M., 2013. Large-Scale control on the Patagonian climate. American Meteorological Society 26, 215–230.

Garret, E., Shennam, I., Watcham, E.P., Woodroffe, S.A., 2013. Reconstructing paleoseismic deformation, 1: modern analogues from the 1960 and 2010 Chilean earthquakes. Quaternary Science Reviews 75, 11–21.

González, H.G., Calderón, M.J., Castro, L., Clement, A., Cuevas, L., Daneri, G., Iriarte, J.L., Lizárraga, L., Martínez, R., Menschel, E., Silva, N., Carrasco, C., Valenzuela, C., Vargas, C.A., Molinet, C., 2010. Primary production and its fate in the pelagic food web of the Reloncaví Fjord and plankton dynamics of the Interior Sea of Chiloé, Northern Patagonia, Chile. Marine Ecology Progress Series 402, 13–30.

Hasle, G.R., Syvertsen, E.E., 1996. Marine diatoms. In: Tomas, C.R. (Ed.), Identifying Marine Diatoms and Dinoflagellates. Academic Press, Inc., San Diego, pp. 5–385.

Hebbeln, D., Marchant, M., Freudenthal, T., Wefer, G., 2000. Surface sediment distribution along the Chilean continental slope related to upwelling and paleoproductivity. Marine Geology 164, 119–137.

Hemphill-Haley, E., 1996. Diatoms as an aid in identifying late-Holocene tsunami deposits. The Holocene 6, 439–448.

Horton, B.P., Sawai, Y., Hawkes, A.D., Witter, R.C., 2011. Sedimentology and paleontology of a tsunami deposit accompanying the great Chilean earthquake of February 2010. Marine Micropaleontology 79, 132–138.

Iriarte, J.L., González, H.E., 2008. Phytoplankton bloom ecology of the Inner Sea of Chiloé, Southern Chile. Nova Hedwigia 133, 67–79.

Iriarte, J.L., González, H.E., Liu, K.K., Rivas, C., Valenzuela, C., 2007. Spatial and temporal variability of chlorophyll and primary productivity in surface waters of southern Chile (41.5–43° S). Estuarine, Coastal and Shelf Science 74, 471–480.

Iriarte, J.L., González, H.E., Nahuelhal., L., 2010. Patagonian fjord ecosystem in southern Chile as a highly vulnerable region: problems and needs. Ambio 39 (7), 436–466.

Jara, I.A., Moreno, P.I., 2012. Temperate rainforest response to climate change and disturbance agents in Northwestern Patagonia (41°S) over the last 2600 years. Quaternary Research 77, 235–244.

Kilian, R., Lamy, F., 2012. A review of Glacial and Holocene paleoclimate records from southernmost Patagonia (49–55°S). Quaternary Science Reviews 53, 1–23.

Kilian, R., Lamy, F., Arz, H., 2013. Late Quaternary variations of the southern westerly wind belt and its influences on aquatic ecosystems and glacier extend within the southernmost Andes. German Journal of Geosciences 164, 279–294.

Lamy, F., Ruhlemann, C., Hebbeln, D., Wefer, G., 2002. High and low latitude climate control on the position of the southern Peru Chile Current during, the Holocene. Paleoceanography 17 (2).

Lamy, F., Kilian, R., Arz, H.W., Francois, J.P., Kaiser, J., Prange, M., Steinke, T., 2010. Holocene changes in the position and intensity of the southern westerly wind belt. Nature Geoscience 3, 695–699.
Lange, D., Cembrano, J., Rietbrock, A., Haberland, C., Dahm, T., Bataille, K., 2008. First seismic record for intra-arc strike–slip tectonics along the Liquiñe-Ofqui fault zone at the obliquely convergent plate margin of the southern Andes. Tectonophysics 455, 14–24.
Lara, A., Villalba, R., Urrutia, R., 2008. A 400-year tree-ring record of the Puelo River summer–fall streamflow in the Valdivian Rainforest eco-region. Climate Change 86, 331–356.
Legrand, D., Barrientos, S., Bataille, K., Cembrano, J., Pavez, A., 2011. The fluid-driven tectonic swarm of Aysén Fjord, Chile (2007) associated with two earthquakes (Mw = 6.1 and Mw = 6.2) within the Liquiñe-Ofqui Fault Zone. Continental Shelf Research 31, 154–161.
León-Muñoz, J., Marcé, R., Iriarte, J.L., 2013. Influence of hydrological regime o fan Andean river on salinity, temperature and oxygen in a Patagonian fjord, Chile. New Zealand Journal of Marine and Freshwater Research http://dx.doi.org/10.1080/00288330.2013.802700.
Marín, J., 2014. Reconstruction of the exported siliceous productivity in the Reloncaví fjord (41 S, 72 W), Chilean Patagonia. Undergraduate thesis, Marine Biology, University of Concepción, Chile 57 pp.
Mayr, C.C., Försterra, G., Häussermann, V., Wunderlich, A., Grau, J., Zieringer, M., Altenbach, A.V., 2011. Stable isotope variability in a Chilean fjord food web: implications for N- and C-cycles. Marine Ecology Progress Series 428, 89–104.
Mayr, C.C., Rebolledo, L., Schulte, K., Schuster, A., Zolitschka, B., Fösterra, G., Häusserman, V., 2014. Responses of nitrogen and carbon deposition rates in Comau Fjord (42°S, Southern Chile) to natural and anthropogenic impacts during the last century. Continental Shelf Research 78, 29–38.
Mazzullo, J., Gilbert, A., Rabinowitz, P., Meyer, A., Garrison, L., 1988. Handbook for Shipboard Sedimentologists (67 pp.).
McCormac, F.G., Hogg, A.G., Blackwell, P.G., Buck, C.E., Higham, T.F.G., Reimer, P.J., 2004. SHCal04 Southern Hemisphere calibration, 0–11 Cal kyr B.P. Radiocarbon 46, 1087–1092.
McQuoid, M.R., Nordberg, K., 2003. Environmental influence on the diatom andsilicoflagellate assemblages in Koljö fjord (Sweeden) over the last two centuries. Estuaries 26, 927–937.
Meyers, P.A., 1997. Organic geochemical proxies of paleoceanographic paleolimnologic and paleoclimatic processes. Organic Geochemistry 27, 213–250.
Moernaut, J., Van Deele, M., Heirman, K., Fontjin, K., Strasser, M., Pino, M., De Batist, M., 2014. Lacustrine turbidites as tool for quantitative earthquake reconstruction: new evidence for a variable rupture model in south central Chile. Journal of Geophysical Research, Solid Earth 119. http://dx.doi.org/10.1002/2013jb010738.
Mohtadi, M., Romero, O.E., Kaiser, J., Hebbeln, D., 2007. Cooling of the southern high latitudes during the Medieval Period and its effect on ENSO. Quaternary Science Reviews 26, 1055–1066.
Montade, V., Nebout, N.C., Chapron, E., Mulsow, S., Abarzúa, A.M., Debret, M., Foucher, A., Desmet, M., Winiarski, T., Kiessel, C., 2012. Regional vegetation and climate changes during the last 13 Kyr from a marine pollen record in Seno Reloncaví, southern Chile. Review of Palaeobotany and Palynology 181, 11–21.
Montero, P., Giovani, G., González, H.E., Iriarte, J.L., Tapia, F.J., Lizárraga, L., Sánchez, N., Pizarro, O., 2011. Seasonal variability of primary production in a fjord ecosystem of the Chilean Patagonia: implications for the transfer of organic carbon within pelagic food webs. Continental Shelf Research 31, 202–215.
Moreno, P.I., Vilanova, I., Villa-Martínez, R., Garreaud, R.D., Rojas, M., De Pol-Holz, R., 2014. Soutern Annular Mode-like changes in southwestern Patagonia at centennial timescales over the last three millenia. http://dx.doi.org/10.1038/ncomms5375.
Mortlock, R., Froelich, P., 1989. A simple method for the rapid determination of biogenic opal in pelagic marine sediments. Deep-Sea Research 36, 1415–1426.
Naranjo, J.A., Arenas, M., Clavero, J., Muñoz, O., 2009. Mass movement-induced tsunamis effects during Patagonian fjordland seismic crisis in Aisen (45°25′ S), Chile. Andean Geology 36 (1), 137–145.
Olsen, J., Rasmussen, P., Heinemeier, J., 2009. Holocene temporal and spatial variation in the radiocarbon reservoir age of three Danish fjords. Boreas 38, 458–470.
Perdue, E.M., Koprivnjak, J.F., 2007. Using the C/N ratioto estimate terrigenous inputs of organic matter to aquatic environments. Estuarine, Coastal and Shelf Science 73, 65–72.
Quintana, J., Aceituno, P., 2012. Changes in the rainfall regime along the extratropical west coast of South America (Chile): 30–43° S. Atmosfera 25 (1), 1–22.
Rebolledo, L., Lange, C.B., Figueroa, D., Pantoja, S., Muñoz, P., Castro, R., 2005. 20th century fluctuations in the abundance of siliceous microorganisms preserved in the sediments of the Puyuhuapi Channel (44°S), Chile. Revista Chilena de Historia Natural 78 (3), 469–488.
Rebolledo, L., Sepúlveda, J., Lange, C., Pantoja, S., Bertrand, S., Hughen, K., Figueroa, D., 2008. Late Holocene marine productivity changes in Northern Patagonia-Chile inferred from a multi-proxy analysis of Jacaf channel sediments. Estuarine, Coastal and Shelf Science 80, 314–322.
Rebolledo, L., González, H.E., Muñoz, P., Iriarte, J.L., Lange, C.B., Pantoja, S., Salamanca, M., 2011. Siliceous productivity changes in Gulf of Ancud sediments (42°S, 72°W), southern Chile, over the last ~150 years. Continental Shelf Research 31, 356–365.
Rebolledo, L., Lange, C., Muñoz, P., Salamanca, M., 2014. Geochemical evidence of past earthquakes in sediments of Reloncaví fjord (Chilean Patagonia) during the last ~ 1000 years. Geophysical Research Abstract EGU2014–15575.
Rivera, P., 1981. Beiträge zur Taxonomie und Verbreitung der Gattung Thalassiosira Cleve. Bibliotheca Phycologica 56, 1–220.
Round, E.E., Crawford, R.M., Mann, D.G. (Eds.), 1990. The Diatoms: Biology and Morphology of the Genera. Cambridge University Press, Cambridge (747 pp.).
Sancetta, C., Villareal, T., Falkowski, P., 1991. Massive fluxes of Rhizosolenid diatoms: a common ocurrence? Limnology and Oceanography 36 (7), 1452–1457.
Schrader, H., Gersonde, S., 1978. Diatoms and silicoflagellates in the eight meters section of the lower Pliocene on Campo Rosello. Utrecht Micropaleontological Bulletin 17, 129–176.
Sepúlveda, J., Pantoja, S., Hughen, K., Lange, C., González, F., Muñoz, P., Rebolledo, L., Castro, R., Contreras, S., Ávila, A., Rossel, P., Lorca, G., Salamanca, M., Silva, N., 2005. Fluctuations in export productivity over the last century from sediments of a southern Chilean fjord (44°S). Estuarine, Coastal and Shelf Science 65, 587–600.
Sepúlveda, J., Pantoja, S., Hughen, K.A., Bertrand, S., Figueroa, D., León, T., Drenzek, N.J., Lange, C.B., 2009. Late Holocene sea-surface temperature and precipitation variability in northern Patagonia, Chile (Jacaf Fjord, 44°S). Quaternary Research 72 (3), 400–409.
Sepúlveda, J., Pantoja, S., Hughen, K.A., 2011. Sources and distribution of organic matter in northern Patagonian fjords, Chile (~44–47°S): a multi-tracer approach for carbon cycling assessment. Continental Shelf Research 31, 315–329.
SERNAGEOMIN, 2003. Mapa geológico de Chile, versión digital, escala 1:100.000.
Shindell, D.T., Schmidt, G.A., 2004. Southern Hemisphere climate response to ozone changes and greenhouse gas increases. Geophysical Research Letters 31, L18209. http://dx.doi.org/10.1029/2004GL020724.
Sievers, H., Silva, N., 2008. Water masses and circulation in austral Chilean channels and fjords. In: Silva, N., Palma, S. (Eds.), Progress in the oceanographic knowledge of Chilean interior waters, from Puerto Montt to Cape Horn. Comité Oceano-gráfico Nacional-Pontificia Universidad Católica de Valparaíso, Valparaíso, pp. 53–58.
Silva, N., Prego, R., 2002. Carbon and Nitrogen spactial segregation and stoichiometry in the surface sediments of Southern Chilean Inlets (41°–56° S). Estuarine, Coastal and Shelf Science 55, 763–775.
Silva, N., Haro, J., Prego, R., 2009. Metals background and enrichment in the Chiloé Interior Sea sediments (Chile). Is there any segregation between fjords, channels and sounds? Estuarine, Coastal and Shelf Science 82, 469–476.
Silva, N., Vargas, C.A., Prego, R., 2011. Land–ocean distribution of allocthonous organic matter in the surface sediments of the Chiloé and Aysén interior seas (Chilean Northern Patagonia). Continental Shelf Research 31, 330–339.
Sims, P.A. (Ed.), 1996. An Atlas of British Diatoms. Biopress Ltd, Bristol United Kingdom (601 pp.).
St-Onge, G., Chapron, E., Mulsow, S., Salas, M., Viel, M., Debret, M., Foucher, A., Muldert, T., Winiarski, T., Desmet, M., Costa, P.J.M., Ghaleb, B., Jaouen, A., Locat., J., 2012. Comparison of earthquake-triggered turbidites from the Saguenay (Eastern Canada) and Reloncaví (chilean margin) Fjords: implications for paleoseismicity and sedimentology. Sedimentary Geology 243–244, 89–107.
Thornton, S.F., McManus, J., 1994. Application of organic carbon and nitrogen stable isotope and C/N ratios as source indicators of organic matter provenance in estuarine systems: evidence from the Tay Estuary, Scotland. Estuarine, Coastal and Shelf Science 38, 219–233.
Tréguer, P.J., De la Rocha, C.L., 2013. The world ocean silica cycle. Annual Review of Marine Science 5, 477–501.
Turekian, K., Cochran, K., Benninger, L., Aller, R., 1980. The sources and sinks of nuclides in Long Island Sound. Advances in Geophysics 22, 129–163.
Valle-Levinson, A., Sarkar, N., Sanay, R., Soto, D., León, J., 2007. Spatial structure of hydrography and flow in Chilean Fjord, Estuario Reloncaví. Estuaries and Coasts 30 (1), 113–126.
Van Daele, M., Versteeg, W., Pino, M., Urrutia, R., De Batist, M., 2013. Widespread deformation of basin-plain sediments in Aysén fjord (Chile) due impact by earthquake-triggered, onshore-generated mass movements. Marine Geology 337, 67–79.
Vargas, C.A., Martínez, R.A., San Martín, V., Aguayo, M., Silva, N., Torres, R., 2011. Allochthonous subsidies of organic matter across a lake–river–fjord landscape in the Chilean Patagonia: implications for marine zooplankton in inner fjord areas. Continental Shelf Research 31, 187–201.
Vargas, G., Rebolledo, S., Sepúlveda, S., Lahsen, A., Thiele, R., Townley, B., Padilla, C., Rauld, R., Herrera, M., Lara, M., 2013. Submarine earthquake rupture, active faulting and volcanism along the major Liquiñe-Ofqui Fault Zone and implications for seismic hazard assessment in the Patagonian Andes. Andean Geology 40 (1), 141–171.
Villalba, R., Lara, A., Masiokas, M.H., Urrutia, R., Luckman, B.H., Marshall, G.J., Mundo, I.A., Christie, D.A., Cook, E.R., Neukom, R., Allen, K., Fenwick, P., Boninsegna, J.A., Srur, A.M., Morales, M.S., Araneo, D., Palmer, J.G., Cuq, E., Aravena, J.C., Holz, A., LeQuesne, C., 2012. Unusual Southern Hemisphere tree growth patterns induced by changes in the Southern Annular Mode. Nature Geoscience 5, 793–798.
Watt, S.F.L., Pyle, D.M., Naranjo, J.A., Mother, T.S., 2009. Landslide and tsunami hazard at Yate volcano, Chile as an example of edifice destruction on strike–slip fault zones. Bulletin of Volcanology 71, 559–574.
Witkowski, A., Lange-Bertalot, H., Metzeltin, D., 2000. Diatom flora of marine coast I. Diversity taxonomy-identificationIconographia diatomologica annotated diatom micrographs Vol. 7. Koeltzs Scientific Books, Königstein, Germany (925 pp.).